A DEEP LEARNING APPROACH FOR ESTIMATING AND PROJECTING GROSS PRIMARY PRODUCTIVITY IN ETHIOPIA UNDER SHARED SOCIOECONOMIC PATHWAY SCENARIOS

ANTENEH, B.[1#] – DHAKAL, T.[1#] – KIM, T.-S.[1#] – TIWARI, S.[1] – KIM, J.-Y.[1] – JANG, G.-S.[1*] – LEE, Y.[2,3*]

[1]*Department of Life Sciences, Yeungnam University, Gyeongbuk 38541, Republic of Korea*

[2]*Department of Agriculture, Forestry and Bioresources Seoul National University, Seoul 08826, Republic of Korea*

[3]*Research Institute of Agriculture and Life Sciences, Seoul National University, Seoul 08826, Republic of Korea*

[#]*These authors contributed equally to this work*

**Corresponding authors*
e-mail: sunside@ynu.ac.kr (G.-S. Jang); johnlee@snu.ac.kr (Y. Lee)

(Received 2nd Oct 2025; accepted 22nd Jan 2026)

Abstract. Understanding the impact of climate change on ecosystems is essential for effective environmental planning and resource management, particularly in sensitive tropical regions. This study explored the impact of climate change on Gross Primary Productivity (GPP), a key indicator of the carbon cycle, in a tropical region with high biodiversity and climate sensitivity in Ethiopia. By leveraging deep learning long short-term memory (LSTM) networks, we captured the complex nonlinear interactions between climate variables and vegetation productivity. We integrated historical climate data, satellite-derived GPP estimates, and projected the Coupled Model Intercomparison Project (CMIP6)-based Shared Socioeconomic Pathways (SSPs) and carbon dioxide (CO_2) emission scenarios (SSP1-2.6, SSP2-4.5, SSP3-7.0, SSP5-8.5) under six Earth System Models (ESMs). The growth of GPP per decade was expected to increase by 12.34 ± 8.01, 36.71 ± 15.79, 65.48 ± 21.61, and 89.79 ± 27.28 percent (%) under the SSP1-2.6, SSP2-4.5, SSP3-7.0, and SSP5-8.5 scenarios, respectively, by 2100, based on the Multimodal Ensemble Mean (MEM) of ESMs. The spatial distribution of GPP in the study area revealed higher values in the southwestern mid-latitude (7-11 degree) and lower values in the northeast high-latitude (11-15 degree) zones. The approach and findings of this study would respond to the anticipated climate change, putting into practice an integrated sustainable management plan to create a green economy in Ethiopia and contribute to the net-zero emissions and climate resilient mission of global sustainable development goals (SDGs).
Keywords: *deep learning, earth system models, spatio-temporal variations, shared socio-economic pathways, tropical zone*

Introduction

Global climate change is a significant threat to life on Earth, due to altering vegetation dynamics, increasing both carbon emissions and global average temperature (Ghazi et al., 2025; Gottfried et al., 2012; Wei et al., 2024; Yuan et al., 2021). According to Intergovernmental Panel on Climate Change (IPCC) Assessment Reports (AR6), the global mean surface temperature is projected to reach around 1.5°C above pre-industrial levels in the early 2030s under all scenarios, and could exceed 2°C by the end of the 21st century unless strong and sustained reductions in greenhouse gas emissions are achieved (Chen, 2021; Kong et al., 2022). Terrestrial vegetation plays a key role in the regulation of climate change and carbon sequestration (Getachew Mengistu et al., 2021; Nolan et al., 2018; Pan et al., 2015; Zhao et al., 2024). GPP is a fundamental process in the Earth's carbon cycle

http://www.aloki.hu ● ISSN 1589 1623 (Print) ● ISSN 1785 0037 (Online)
DOI: http://dx.doi.org/10.15666/aeer/2402_31173147

(Lu et al., 2024; Wang et al., 2024a) and it is one of the main controlling variables of biosphere-climate interactions, hydrological cycles, and carbon budget (Park and Jeong, 2021). GPP is expressed as the atmospheric CO_2 captured by plant photosynthesis (Qian et al., 2024), which mediates global climate change (Lu et al., 2023; Wang et al., 2021; Zhou et al., 2017) and expressed as grams of carbon per unit area per unit time (g C m^{-2} yr^{-1}). Globally about thirty percent of human-induced emissions of CO_2 are absorbed by terrestrial ecosystems (Fang et al., 2024; Reichstein et al., 2013; Wu et al., 2024).

Projected warming induces changes in terrestrial vegetation in tropical regions (Allen et al., 2024; Shi et al., 2025; Smith et al., 1992; Wen et al., 2019). Ethiopia is a tropical country vulnerable to climate change and projected warming is expected to induce changes in terrestrial vegetation in tropical regions. Therefore, monitoring the spatial and temporal vegetation dynamics is important for regulating global climate change and reducing CO_2 emissions (Bai et al., 2023; DeAngelo et al., 2021). Ethiopia established a climate resilience and green economy strategy (CRGE) (Climate Action Tracker, 2020; Dagne et al., 2023). The spatiotemporal variation in GPP mainly depends on climate variables (Jacob et al., 2020). Precipitation and temperature are the main climate factors that significantly influence carbon sequestration efficiency (Cao et al., 2021; Guo et al., 2021; He et al., 2015; Xie et al., 2016) Recent years, vegetation dynamics studies in Ethiopia lack timeseries accurate quantification of projected GPP in future climate scenarios using high precision machine learning algorithms (Ugbaje et al., 2017). Most studies have conducted spatiotemporal analyses of vegetation productivity response to climate change at global and regional levels (Wang et al., 2023). However, studies in tropical regions, such as Ethiopia, that project vegetation productivity responses to climate change under future climate scenarios are very limited (Khalifa et al., 2018). Accurate quantification of GPP is critical for regulating and monitoring the Earth's carbon cycle, ecosystem growth and carbon sequestration potential for future climate change investigation (Zhang et al., 2024b).

Machine learning is an effective strategy for examining climate-induced spatial properties (Li et al., 2024; Montero et al., 2024; Xiong et al., 2024). non-process-based machine learning technique LSTM networks are the variants of the Recurrent Neural Network (RNN) architecture mostly applied for processing nonlinear, complex, and long-time-series datasets (Al Mehedi et al., 2023; Guo et al., 2024). This study aimed to assess spatiotemporal variations and forecast GPP trend from CMIP6 datasets under different Shared Socioeconomic Pathways (SSPs) scenarios in Ethiopia. We examined GPPs for the near future (2015 to 2060) and far future: the end of century (2061 to 2100) from the historical baseline of 1982 to 2014 global GPP data under climatic scenarios applying LSTM networks. The study provides valuable insights for estimated GPP into unique ecological tropical zone Ethiopia and supports on designing the policies on CO_2 sequestration and climate change mitigation strategies for achieving global SDGs.

Materials and methods

Research area

The study was conducted in Ethiopia, which is in the East African tropical climate region located between 33°–48° E and 3°–15° N (*Fig. 1a*). The country's elevation ranges from the Afar Depression (~125 m below sea level) in the east to the spectacular world heritage site Simien Mountain (4326 m above sea level) in the north. The diversity of climate and topographic variability in Ethiopia causes precipitation and temperature to be

http://www.aloki.hu ● ISSN 1589 1623 (Print) ● ISSN 1785 0037 (Online)
DOI: http://dx.doi.org/10.15666/aeer/2402_31173147

spatially and temporally dynamic across the region (Rettie et al., 2023). The spatial annual temperature ranges from 12.5-30.0°C, with an average of 22.90°C, and precipitation from 200 to 1600 mm (760.67 mm/yr) in the low and higher elevation areas (Getnet et al., 2023; Tesfaye et al., 2025) (*Fig. 1c, d*). These spatial-temporal distributions of climate were governed by the movement of the Intertropical Convergence Zone (ITCZ) between the Equator and Tropic of Cancer (Almazroui et al., 2020; Assfaw et al., 2023; Berihun et al., 2023; Luhunga, 2025). The spatial annual GPP between 1982 to 2014 was ranges from 200 to 1600 g C m^{-2} yr^{-1} (Kayiranga et al., 2022; Lomax et al., 2024), with an average of 482.74 g C m^{-2} yr^{-1}, as indicated in density distribution plot (*Fig. 1b*).

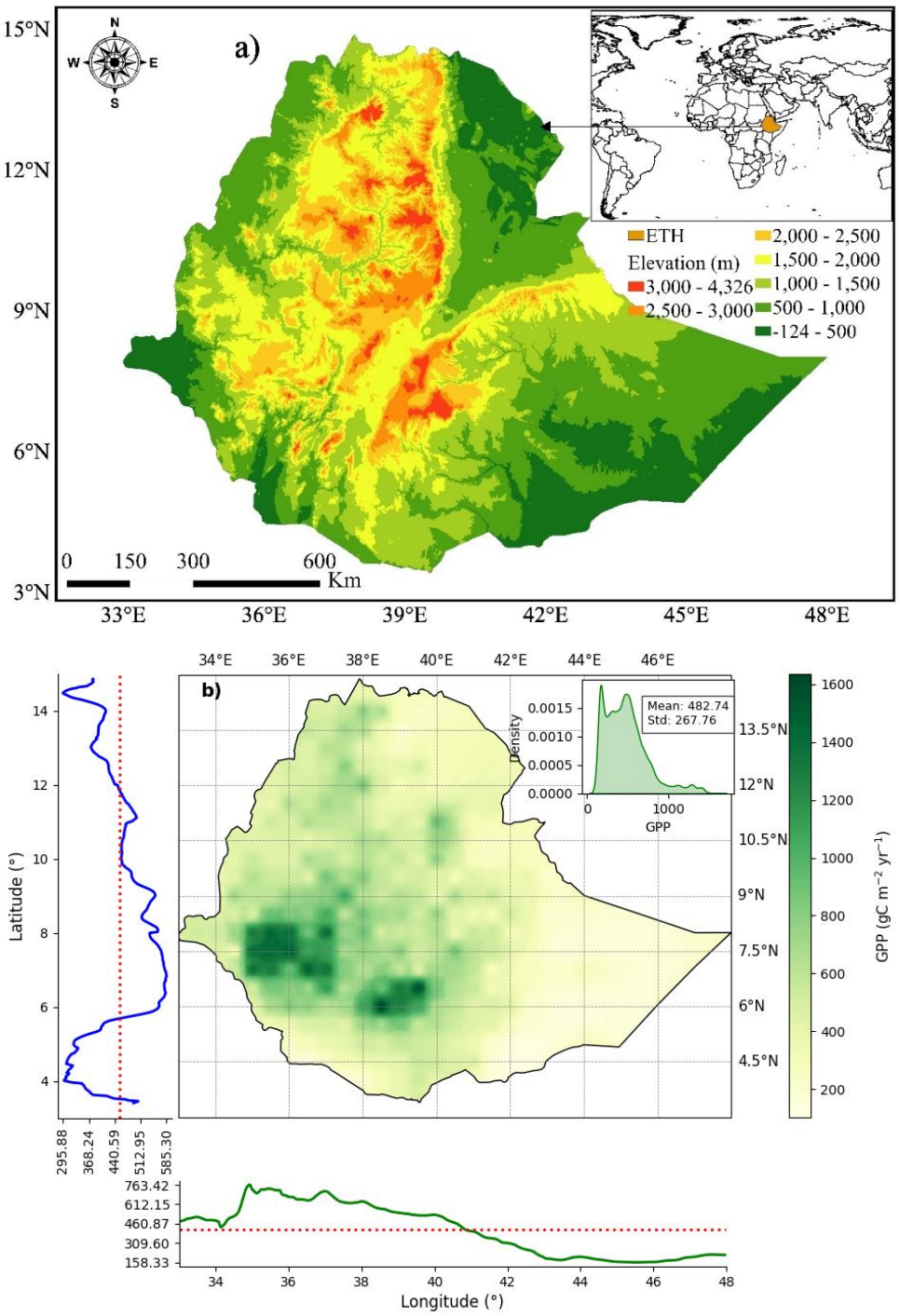

http://www.aloki.hu ● ISSN 1589 1623 (Print) ● ISSN 1785 0037 (Online)
DOI: http://dx.doi.org/10.15666/aeer/2402_31173147

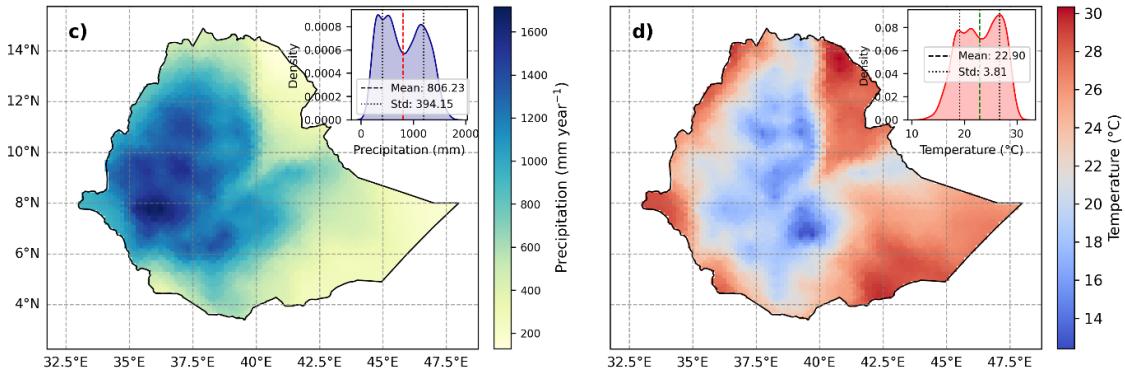

Figure. 1. *Survey area (a) elevation map produced by using ArcGIS Pro, and annual mean of (b) GPP, (c) precipitation and (d) temperature between 1982 to 2014 using python*

Data sources

In this study, monthly GPP from an improved light use efficiency model was used as observation data from 1982 to 2014 (https://daac.ornl.gov/cgi-bin/dsviewer.pl?ds_id=1789), with monthly temporal resolution and 0.083° spatial resolution, and then resampled to 0.5° resolution to ensure consistency with the observed climate variables. For GPP simulations, we used a process-based light-use efficiency model (Shao et al., 2025), that has advantages over others for predicting GPP dynamics with consistent climate variables (Bi et al., 2022; Zhang et al., 2015).

Similarly, historical temperature and precipitation (climatic data) were extracted from the Climate Research Unit Time Series version 4.00 (CRU TS v4.00) from 1901 to 2015 at 0.5°× 0.5° grid resolution from the UK National Center for Atmospheric Science (Harris et al., 2020; Yuxi et al., 2024) and sliced for 1982 to 2014 mapping to the study region. To explore the latitudinal and altitudinal variation we mapped with the Digital Elevation Model (DEM) data that extracted from NOAA at a spatial resolution of 1 km (https://www.ncei.noaa.gov/products/etopo-global-relief-model) (Zhang et al., 2023).

The ESMs climate datasets were obtained from CMIP6 archives with the same variant label r1i1p1f1 (where, '*r*' realization, '*i*' initialization, '*p*' physics, and '*f*' forcing) (Eyring et al., 2016). The monthly climatic data (https://esgf-node.ornl.gov/search) were used to reduce differences among six ESM models under four SSP scenarios (SSP1-2.6, SSP2-4.5, SSP3-7.0, SSP5-8.5). These four SSPs represent sustainable low-emission development (SSP1-2.6), middle-of-the-road development with intermediate emissions (SSP2-4.5), uneven regional development with medium-to-high emissions (SSP3-7.0), and fossil-fuel-driven development with high emissions (SSP5-8.5) scenarios (Meinshausen et al., 2020; Riahi et al., 2017). We select six representative ESM models (*Table 1*) based on full availability of historical and future SSPs for all variables, suitable for model simulating study in Ethiopian vegetation and climate variability (Berhanu et al., 2025; Makula and Zhou, 2022). The CMIP6 climate dataset monthly temperature, precipitation, and GPP (for comparison purposes) were further processed into annual averages to perform ensemble model simulations to minimize the uncertainty (Fan et al., 2020). The selected monthly climate variables temperature and precipitation extracted from CMIP6 models and computed annually using arithmetic mean of Multimodal Ensemble Mean (MEM) ESMs simulations (Song et al., 2021) to minimize uncertainty (*Fig. A1*).

http://www.aloki.hu ● ISSN 1589 1623 (Print) ● ISSN 1785 0037 (Online)
DOI: http://dx.doi.org/10.15666/aeer/2402_31173147

Table 1. *List of CMIP6 ESM models used for this study*

Model name	Institution	Resolution (Lon × Lat)	Reference
BCC-CSM2-MR	BCC, China	1.1° × 1.1°	Azad and Ahmadi (2024)
CanESM5	CCCMA, Canada	2.8° × 2.8°	Almazroui et al. (2021a)
CMCC-ESM2	CMCC, Italy	1.2° × 0.9°	Enyew et al. (2024)
CMCC-CM2-SR5	CMCC, Italy	1.3° × 0.9°	Firpo et al. (2022)
CAS-ESM2-0	CAS, China	1.4° × 1.4°	Zhang et al. (2020)
TaiESM1	AS-RCEC, Taiwan	1.3° × 1.0°	Almazroui et al. (2021b)

Processing CMIP6 ESMs climate dataset

The selected ESMs data have different spatial resolutions that cannot be directly used in process models (Alkama et al., 2022; Anav et al., 2013; Gidden et al., 2019; Wang and Tian, 2024). Therefore, to handle uncertainty (Ossó et al., 2023) and simplicity, MEM of all ESM models was computed with a common spatial resolution of 1°. Statistical downscaling (SD) analysis to smooth grid differences (Fauzi et al., 2020) using bilinear interpolation was applied to reduce errors. Bias corrections (BC) using the Quantile Delta Mapping (QDM) (Cannon et al., 2015; Wang and Tian, 2022) method were applied for consistent observed data and future simulated ensemble ESMs datasets. BC CMIP6 datasets are resampled into 0.5° × 0.5° grid longitude and latitude spatial resolution (Peng et al., 2023). QDM computes the empirical cumulative distribution function (ECDF) and inverse quantile function (CDF) (Gergel et al., 2024; Rettie et al., 2023) of the historical observed bias-corrected projected climate data (Yılmaz et al., 2024), statistically expressed as *Equation 1*:

$$Y_{bc,fut} = F_{obs}^{-1}\left(F_{mod,hist}\left(Y_{mod,fut}\right)\right) + \left(Y_{mod,fut} - Y_{mod,hist}\right) \quad \text{(Eq.1)}$$

where: $F_{bc,fut}$ are bias-corrected future climate variables (precipitation and temperature), $Y_{mod,fut}$ future climate model output, $Y_{mod,hist}$ the historical model climate variable, $F_{mod,hist}$ stands for the empirical cumulative distribution function of the historical period scenario data, F_{obs}^{-1} is the inverse quantile function of the observed climate data.

Long short-term memory networks and trend

Deep learning is a powerful non-process-based machine learning approach for long time series data processing (classification and prediction) spatiotemporally (Chen et al., 2021; Reichstein et al., 2019). In the recent era, RNN deep learning architectures were widely used for data processing and modeling (Lecun et al., 2015). The training process in RNN is problematic because of the vanishing gradient issue (Vasilakos et al., 2022). LSTM networks, the variants of RNN were widely applied for modeling time-series datasets (Guo et al., 2023). LSTM algorithms are suitable for modeling, storing long-term information in internal memory, and addressing vanishing gradient problems in RNN (Graves, 2013). For the prediction of GPP with climatic variables under the SSPs scenarios, we applied the LSTM model (Hochreiter and Schmidhuber, 1997. The spatial-temporal dynamics of Gross Primary Productivity (GPP) were modeled using a LSTM network, guided conceptually by the framework as *Equation 2* (Yang et al., 2022):

$$\mathrm{GPP}_t\,(x,y) = \beta_0 + \beta_1\,P_t(x,y) + \beta_2\,T_t(x,y) + \varepsilon \quad \text{(Eq.2)}$$

http://www.aloki.hu ● ISSN 1589 1623 (Print) ● ISSN 1785 0037 (Online)
DOI: http://dx.doi.org/10.15666/aeer/2402_31173147

where $GPP_t\,(x,y) = \beta_0$ is the average GPP at location *(x, y)* at year *t*, $P_t(x,y), and\ T_t(x,y)$ are the climatic variables (temperature and precipitation), β_0 is the intercept, multipliers β_1 and β_2 are the trend of climatic variables, and ε is the noise. The trend is increasing if the coefficient is positive; otherwise, it decreases. In the context of comparing between variables β_2 is considered zero ($\beta_2 = 0$) while examining with *P*, and β_1 is zero ($\beta_1 = 0$) for *T*.

The inter-annual GPP trends were analyzed using the pixel-wise linear slope estimation approach, further we applied t-test for significance of regression slope and projected under the SSP scenario (Anav et al., 2015; Li et al., 2023). The average GPP from 1982 to 2014 was set as baseline data (b_0) for 2014 and was examined percent change trends for the near future 2060 (2015-2060), and the far future 2100 (2061–2100) (b_n) (*Eq. 3*) (Bongasie et al., 2024).

$$GPP = \frac{b_n - b_0}{b_0} * 100\ \forall\ n = 2015, 2016, \ldots.2100 \qquad \text{(Eq.3)}$$

where GPP rate of change, b_n is changes of future average value at different period, b_0 average value from 1982 to 2014 as assuming the data of year 2014.

Model training and validation

The time series spatial data (GPP, T and P) from 1982 to 2014 were normalized to upgrade the model's performance and convergence (Ma et al., 2022). Reliable predictions require that the model can accurately reproduce the variability observed in data during the validation period (Chen et al., 2022; Chin and Lloyd, 2024; Martinuzzi et al., 2024). Accordingly, the normalized dataset was split into training and validation sets: 80% of the data (1982–2008) were used for model training, and the remaining 20% (2009–2014) for validation. The model was performed in Python 3.11.11, Kera's 3.8 and TensorFlow 2.18 environment. The LSTM model was trained using the Adam optimizer up to 100 epochs with a batch size of 32, and an initial learning rate of 0.001 (1×10^{-3}). A linear activation function was employed in the output layer, while the hyperbolic tangent ("tanh") activation was used in the hidden layers to capture nonlinear temporal patterns. To optimize the training, improving the convergence early stopping applied with a patience of 30 epochs prevents gradient problems and overfitting.

The accuracy of the LSTM model fitness was evaluated using the most widely used performance metrics, including the coefficient determination (R^2), root mean square error (RMSE), and mean absolute error (MAE), which were applied to check the performance of the target and simulated datasets in the model (*Eq. 4*). The higher the R^2 and the lower the RMSE and MAE values, the better the model fit and the higher the model accuracy (Li et al., 2023, 2020; Wei et al., 2023; Zhang et al., 2022).

$$MAE = \frac{1}{n}\sum_{i=1}^{n}|y_{obs} - y_{sim}|$$
$$RMSE = \sqrt{\frac{1}{n}\sum_{i=1}^{n}(y_{sim} - y_{obs})^2} \qquad \text{(Eq.4)}$$
$$R^2 = 1 - \frac{\sum_{i=1}^{n}(y_{obs} - y_{sim})^2}{\sum_{i=1}^{n}(y_{obs} - \bar{y}_{obs})^2}$$

http://www.aloki.hu ● ISSN 1589 1623 (Print) ● ISSN 1785 0037 (Online)
DOI: http://dx.doi.org/10.15666/aeer/2402_31173147

where n is the number of samples, simulation GPP is represented by y_{sim}, the reference observed by y_{obs}, and mean of GPP is denoted as $\bar{y}_{obs}$. The graphical presentation of work is summarized in *Figure 2*.

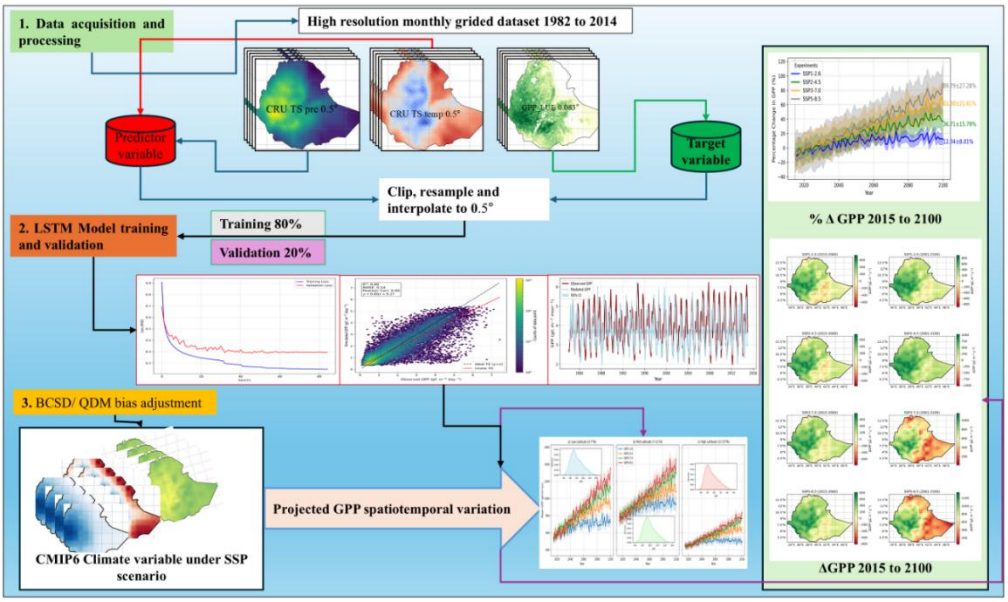

Figure 2. *Graphical framework of study*

Results

Spatiotemporal variation and trends of observed GPP

The spatial trends of historical period GPP value differ across of latitudinal and longitudinal variation. Mean and standard deviations of GPP trend presented in density distribution plot estimated to be 0.19 and 0.34 g C m^{-2} yr^{-1} (*Fig. 3*). The higher GPP values 0.75 g C m^{-2} yr^{-1} are distributed in the mid-altitude 6°N to 8°N southwest region and lower values in the high-latitude 11°N to 15°N northeastern region of Ethiopia extends from -0.75 to 0.75 g C m^{-2} yr^{-1} (*Fig. 3a*). The interannual variation of observed GPP within the time interval from 1982 to 2014 ranged from 700 to 800 g C m^{-2} yr^{-1} with an average of 755.73 g C m^{-2} yr^{-1} (*Fig. 3b*). The trend computed using pixel-level linear regression analysis showed that dynamic changes across the region. When fitting the linear model to time domain, we observed the dynamic value with an overall positive trend (statistically insignificant $R^2 = 0.06 > 0.05$); GPP increased at an annual rate of 0.74 g C m^{-2} yr^{-1}.

The dynamic variation in climate factors and GPP across elevational differences and their trends can be seen in supplementary documents (*Fig. A2*). The relationship between GPP and precipitation showed a positive increasing trend with elevation, but temperature showed a significant negative trend and changed at a rate of 0.004°C/m (*p-value* < 0.05, $R^2 = 0.71$). The rate of change in GPP and precipitation over elevation was 0.19 g C m^{-2} yr^{-1}/m and 0.33 mm yr^{-1}/m with ($R^2 = 0.11$ and 0.35), respectively.

Spatiotemporal variation of climate factors under SSP scenarios

We observed the variation in temporal trends of climatic variables under future SSP scenarios. The mean annual temperature increased by 0.74°C till 2015 from 1982 and using the MEM approach the temperature growth trends will be 1.02°C, 2.30°C, 3.49°C and

http://www.aloki.hu ● ISSN 1589 1623 (Print) ● ISSN 1785 0037 (Online)
DOI: http://dx.doi.org/10.15666/aeer/2402_31173147

4.59°C in SSP1-2.6, SSP2-4.5, SSP3-7.0, and SSP5-8.5 scenarios, respectively by 2100 (*Figs. 4a, A3*). It was observed that the average temperature will be above 2°C at the end of 21th century, the projected warming is likely to exceed < 5%, 32%, 80%, and 99% under the future SSP1-2.6, SSP2-4.5, SSP3-7.0, and SSP5-8.5, respectively (*Table A1*). The trends of temporal average annual precipitation are uncertain under historical and future SSP scenarios owing to the north-south movement of the ITCZ. Similarly, change in precipitation trend per decade from 2015 to 2100 will be expected to rise 14.07 ± 71.58 mm, 12.54 ± 84.12 mm, 19.84 ± 105.69 mm, and 26.48 ± 129.66 mm under SSP1-2.6, SSP2-4.5, SSP3-7.0, SSP5-8.5 scenario, respectively (*Fig. 4b*).

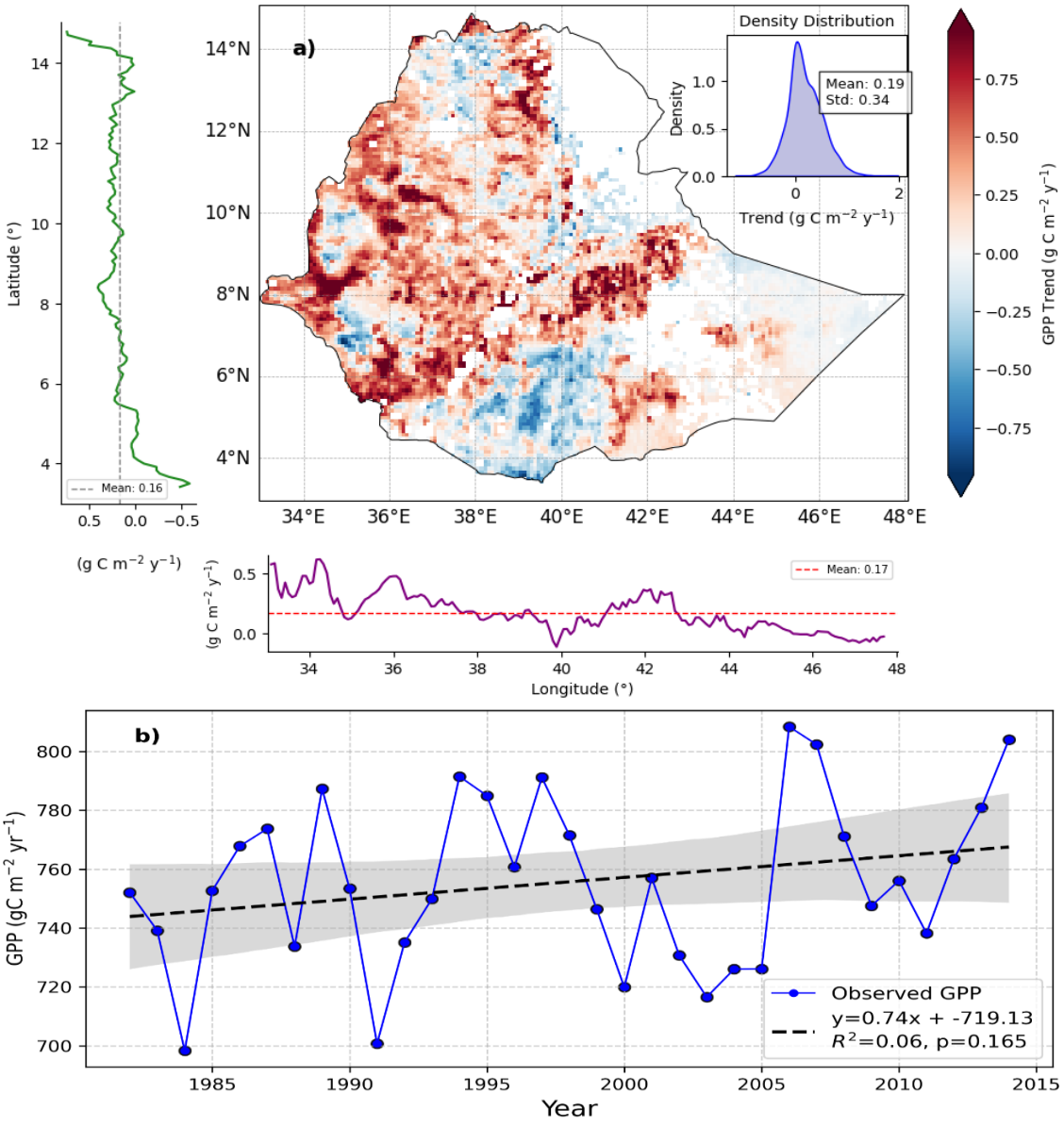

Figure 3. *Spatial distribution of annual GPP trend (a), and interannual variation of GPP (b) in Ethiopia from 1982 to 2014*

The spatial distribution of the change in projected temperature in the near future (2015–2060) and far future (2061–2100) periods relative to the baseline under the four

http://www.aloki.hu ● ISSN 1589 1623 (Print) ● ISSN 1785 0037 (Online)
DOI: http://dx.doi.org/10.15666/aeer/2402_31173147

SSPs scenarios can be seen in *Figure A4a.* The results showed that decadal projected temperatures will counter warming in the tropical regions of Ethiopia. A higher spatial distribution of future temperature will occur in the lower latitude areas of northern, eastern, and central parts of Ethiopia from 10.5°N -13.5°N and 38°E -40°E, while low warming will occur in the southern 33°E to 36°E and south western 4.5°N to 9°N parts of Ethiopia. However, the change in temperature warming continues to expand in the higher latitude area than in the low latitudes (Fan et al., 2020) under the SSP 3-7.0 and SSP 5-8.5 scenarios in the future period 2061–2100.

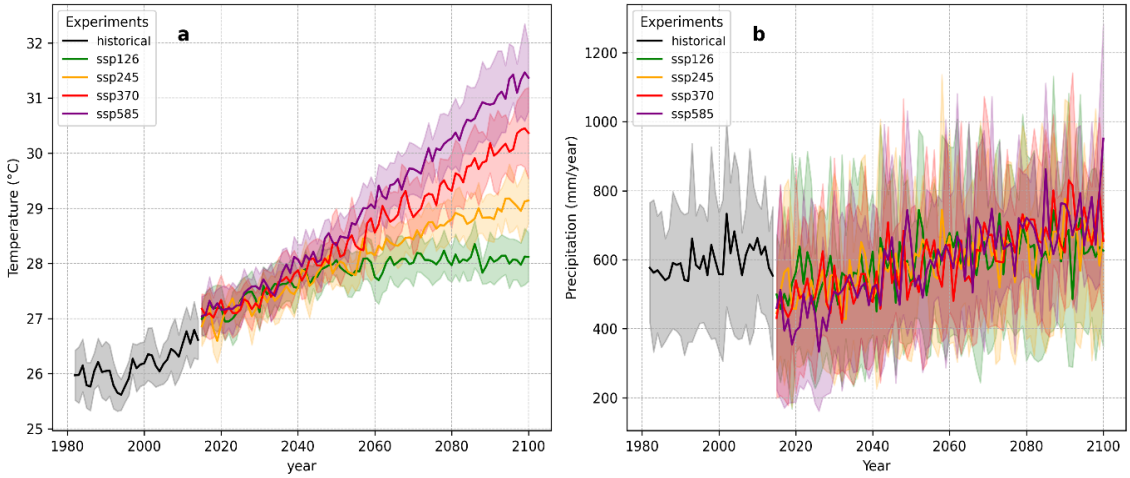

Figure 4. *Temporal change time series annual average temperature and precipitation from 1982 to 2100. The outline of experiments in the MEM 6 ESMs projected temperature and precipitation represents historical (black), SSP 126 (green), SSP245 (yellow), SSP 370 (red), SSP 585 (purple) and the shaded part represents 10th and 90th quantile of standard deviation*

The spatiotemporal trends of future temperature change more specifically from 2015-2060 and 2061-2100, temperature will increase per decade 0.23 ± 0.34°C and 0.03 ± 0.11°C under SSP1-2.6, 0.30 ± 0.42°C and 0.21 ± 0.26°C under SSP2-4.5, 0.37 ± 0.51°C and 0.43 ± 0.52°C under SSP3-7.0, 0.44 ± 0.60°C and 0.59 ± 0.69°C under SSP5-8.5 scenario respectively. The spatial trends of projected warming will be higher in the low-latitude northern and northeastern parts of Ethiopia in both the near- and far-future periods (*Fig. A4b*). The decadal temperature in the southern part will vary from 36°E to 40°E, and a relatively lower warming in the near than far future periods.

The spatial variations in precipitation change in the future SSPs scenarios from 2015-2100 almost similar, but different in intensity (*Fig. A5a*). The higher latitudinal areas of the southwestern and western regions between (6°N -10.5°N) latitude and (34°E–37°E) longitude are associated with higher precipitation distribution. The spatial trends of the projected precipitation will be higher in the mid-high latitude southwestern and central parts of Ethiopia in near future than in far future (*Fig. A5b*). Decadal precipitation is higher in the southwestern part of the region with latitudinal variations from 3°N to 9°N and 33°E to 38°E. Future precipitation decadal trends will decrease from the near future to the far future in SSP1-2.6 and SSP2-4.6 but increase in SSP3-7.0 and SSP5-8.5. The change in projected precipitation decadal value across the study area within the time interval near the future 2015-2060 and far future 2061-2100, precipitation will be expected to decrease per decade from 56.87 ± 71.74 to -1.33 ± 51.38 mm under SSP1-

http://www.aloki.hu ● ISSN 1589 1623 (Print) ● ISSN 1785 0037 (Online)
DOI: http://dx.doi.org/10.15666/aeer/2402_31173147

2.6, 51.26 ± 72.12 to 35.34 ± 62.36 mm under SSP2-4.5, increased from 56.78 ± 71.26 to 61.17 ± 80.76 mm under SSP3-7.0, and a significant increase of 35.61 ± 88.11 mm to 105.40 ± 84.90 mm under the SSP5-8.5 scenarios, respectively.

Model fitness and training efficiency

The LSTM model effectively captured the temporal and spatial variability of the observed datasets, demonstrating its suitability for predictive analysis. *Figure 5* presents the MSE loss curves for the training and validation periods. The loss decreased sharply during the first six epochs, indicating rapid initial learning, and then exhibited moderate fluctuations up to 40 epochs before stabilizing after 60 epochs, confirming the model had reached convergence. The model's predictive performance was high, with coefficients of determination of $R^2 = 0.92$ and 0.80, MAE of 0.46 and 0.34, and RMSE of 0.67 and 0.54 for the training and validation periods, respectively. These metrics indicate that the model reliably reproduced the observed variability in GPP, temperature, and precipitation. Linear regression between simulated and observed historical GPP (inset of *Fig. 5*) further validated the model, showing a significant fit ($R^2 = 0.80$, RMSE = 0.54) with a slope of 0.8. The scatter density analysis revealed that most data points were closely distributed around the ideal fit line, highlighting the model's accuracy, although some points deviated slightly along the positive linear trend, suggesting minor discrepancies in extreme values. Overall, these results confirm that the LSTM model is well-calibrated and capable of generating reliable projections of GPP variability, providing a robust foundation for subsequent predictive analyses.

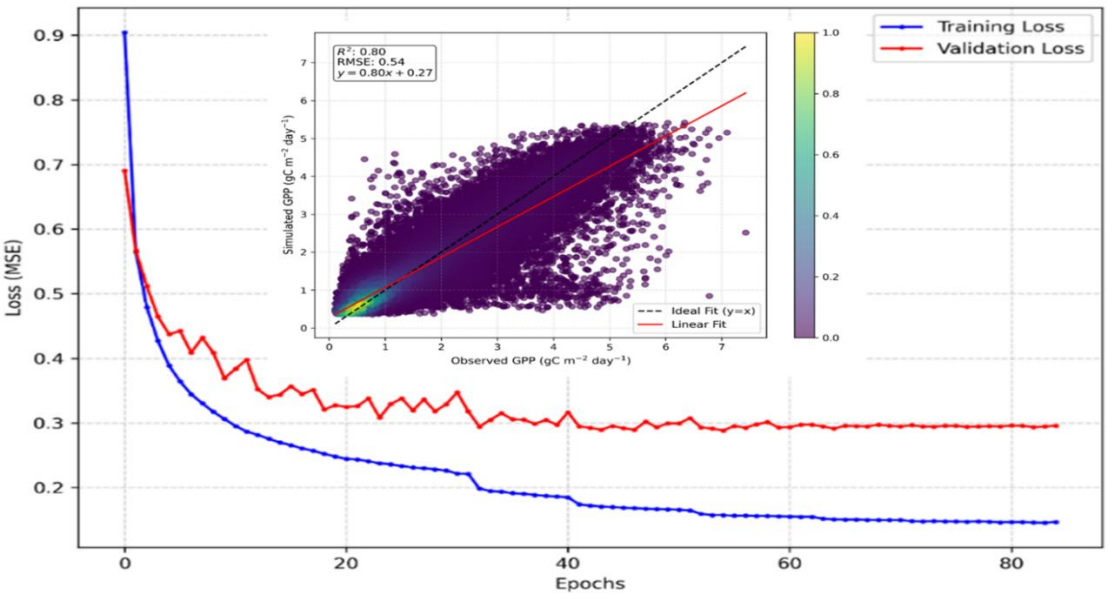

Figure 5. *Model validation graphs: Loss function curve during model training and validation, (inset figure: scatter plot between observed and simulated monthly mean GPP per pixels from 1982 to 2014 (variance ranges in color bar), red line indicates linear and gray dashed lines are ideal fit y = x)*

Spatiotemporal change in GPP

The projected temporal variation of GPP in Ethiopia from the MEM of six ESMs from 2015 to 2100, relative to the baseline period (1982 to 2014), and time series of temporal

http://www.aloki.hu ● ISSN 1589 1623 (Print) ● ISSN 1785 0037 (Online)
DOI: http://dx.doi.org/10.15666/aeer/2402_31173147

mean GPP varied under future SSPs scenarios (*Fig. 6a*). The dynamic spatial pattern of annual GPP in the four SSP scenarios were observed: mid-latitudinal region of southwest parts will experience higher GPP values ranging from latitude 4.5°N - 10.5°N and longitude 33°E - 38°E. The lower (<6°N) and high (>11°N) latitudes northeastern region of Ethiopia will have lower precipitation patterns, and higher temperature in a decrease in GPP value than southwest regions of Ethiopia under all SSPs scenarios (*Fig. 6b*). While observing the spatiotemporal and density distribution of GPP among the examined scenarios, higher concentration in the SSP5-8.5 throughout the 21st century.

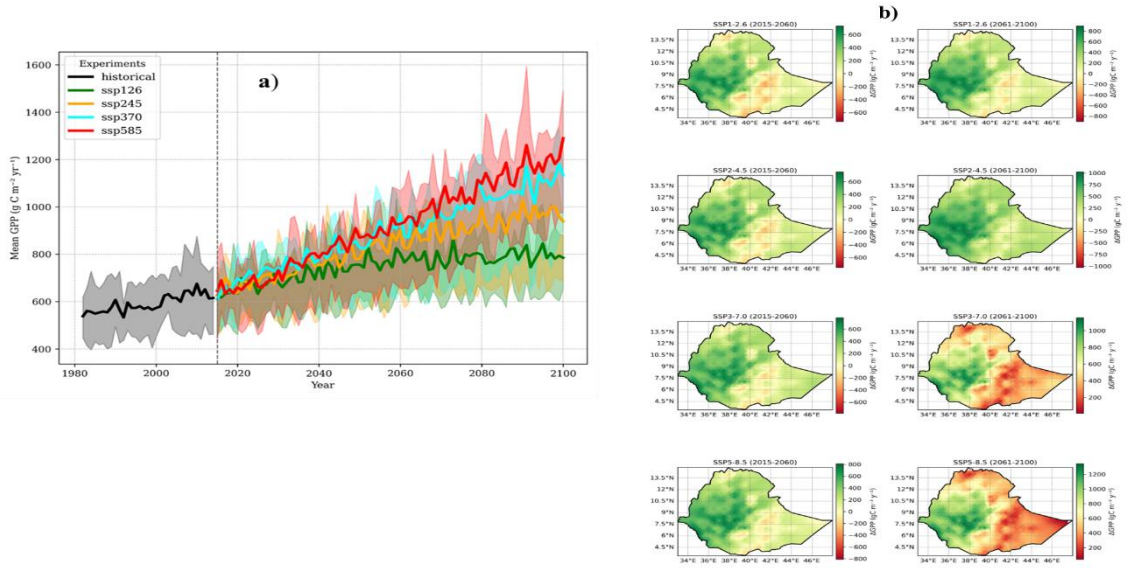

Figure 6. *(a) Temporal annual mean GPP during the period of 1982 to 2100 using six ESM models, the shaded area represents the 25th and 75th percentile. (b) Spatial distribution of annual GPP change between observed 1982-2014, near future 2016-2060 and far-future 2061-2100 under SSP1-2.6, SSP2-4.5, SSP3-7.0, SSP5-8.5 scenarios*

Trends of projected GPP

The trends of projected GPP for the near future (2060) and far future (2100) were quantified using pixel-level linear trends derived from the LSTM model (*Table 2*). The temporal mean GPP exhibited distinct responses across future SSP scenarios, with higher growth rates observed under scenarios with greater fossil fuel–driven CO_2 emissions, particularly SSP5-8.5. By 2060, the projected decadal percentage change in GPP was estimated at 15.30 ± 7.65, 30.03 ± 10.56, 35.12 ± 14.38, and 39.78 ± 12.28 under SSP1-2.6, SSP2-4.5, SSP3-7.0, and SSP5-8.5, respectively. Similarly, by 2100, GPP showed a significant increase across all scenarios, with projected decadal changes of 12.34 ± 4.26, 36.71 ± 7.45, 65.48 ± 11.80, and 89.79 ± 13.93 under SSP1-2.6, SSP2-4.5, SSP3-7.0, and SSP5-8.5, respectively.

It was observed that the mid-latitude areas of the southern and southwestern parts Ethiopia will experience an increasing trend of GPP from the near 2060 to the far future 2100 under SSP2-4.5, SSP3-7.0, and SSP5-8.5, but the decreasing trend in northern and eastern lowland regions (*Fig. 7*). At the end of the 21st century under SSP5-8.5 scenario a significantly higher spatial cumulative density trends of GPP compared to the other scenarios. Whereas SSP1-2.6 showed a decreased trend as 15.30% ± 7.65% in 2060 and

http://www.aloki.hu ● ISSN 1589 1623 (Print) ● ISSN 1785 0037 (Online)
DOI: http://dx.doi.org/10.15666/aeer/2402_31173147

12.34% ± 4.26% in 2100 (*Fig. 7c, d*). Although the long-term mean GPP exhibits a significant increasing trend under all SSP scenarios, the relatively large standard deviations indicate substantial temporal and spatial variability. This variability implies intermittent and localized declines in primary production during the forecast periods (2015–2060 and 2015–2100), superimposed on the overall increasing trend. Such fluctuations likely reflect climate-driven variability and extreme events captured by the model. The distribution of mean, standard deviation, and interquartile range of percentage changes in GPP relative to the baseline period (2015) is illustrated in boxplots (*Fig. 7a, b*), further highlighting the increasing median trends alongside widening variability under higher-emission scenarios.

The GPP was examined from LSTM network comparing the climatic variables observed from the MEM of ESMs under four carbon emission scenarios: SSP1-2.6, SSP2-4.5, SSP3-7.0, and SSP5-8.5 from 2015 to 2100 (*Fig. 8*). The inter-annual variations in simulated GPP for the six ESMs and MEM indicate a gradual increase in all SSPs scenarios.

Table 2. *The changes in GPP under four SSP scenarios*

Baseline GPP* = 632.31 g C m^{-2}	Absolute % change of GPP		% change in average GPP			Remark
	2060	2100	2015-2060	2061-2100	2015-2100	*p*-value
SSP1-2.6	15.30 ± 7.65	12.34 ± 4.26	3.14 ± 7.7	13.07 ± 4.3	7.76 ± 8.0	<0.05
SSP2-4.5	30.03 ± 10.56	36.71 ± 7.45	8.09 ± 10.6	34.15 ± 7.4	20.47 ± 15.8	<0.05
SSP3-7.0	35.12 ± 14.38	65.48 ± 11.80	12.66 ± 12.3	48.49 ± 11.8	29.32 ± 21.6	<0.05
SSP5-8.5	39.78 ± 12.28	89.79 ± 13.93	12.99 ± 14.4	59.54 ± 13.9	34.64 ± 27.3	<0.05

*Annual average GPP from 1982 to 2014

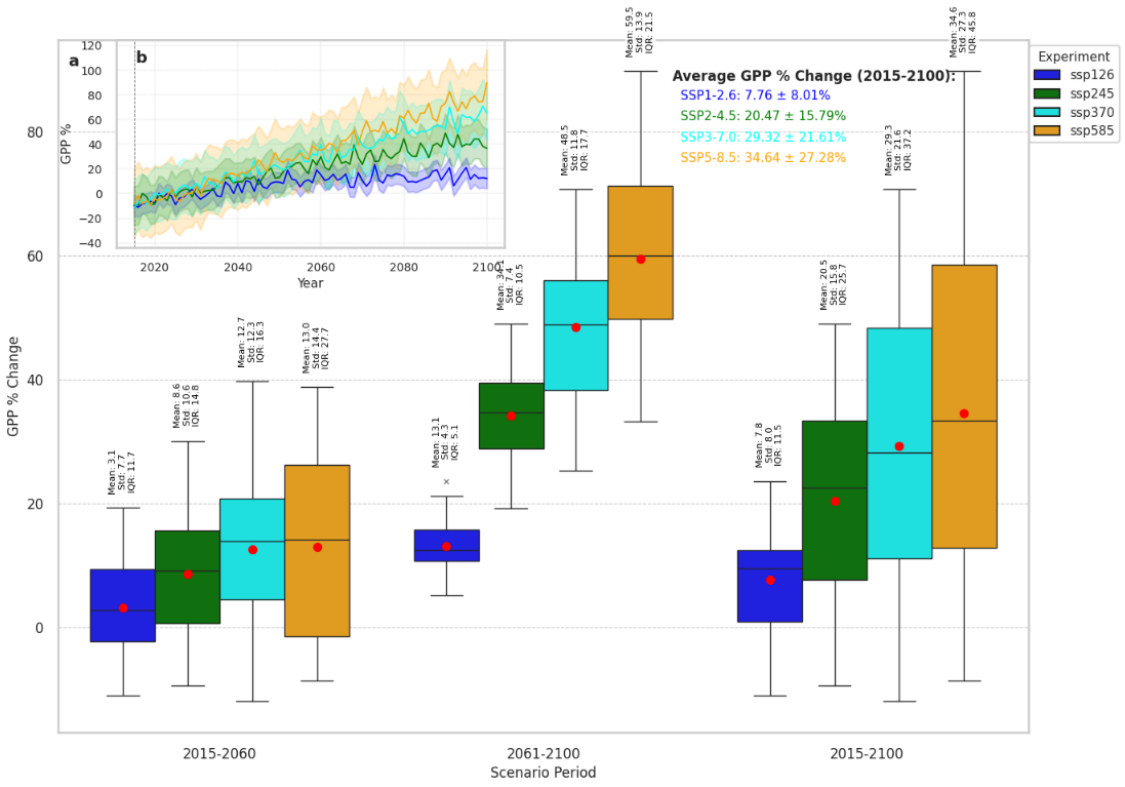

http://www.aloki.hu ● ISSN 1589 1623 (Print) ● ISSN 1785 0037 (Online)
DOI: http://dx.doi.org/10.15666/aeer/2402_31173147

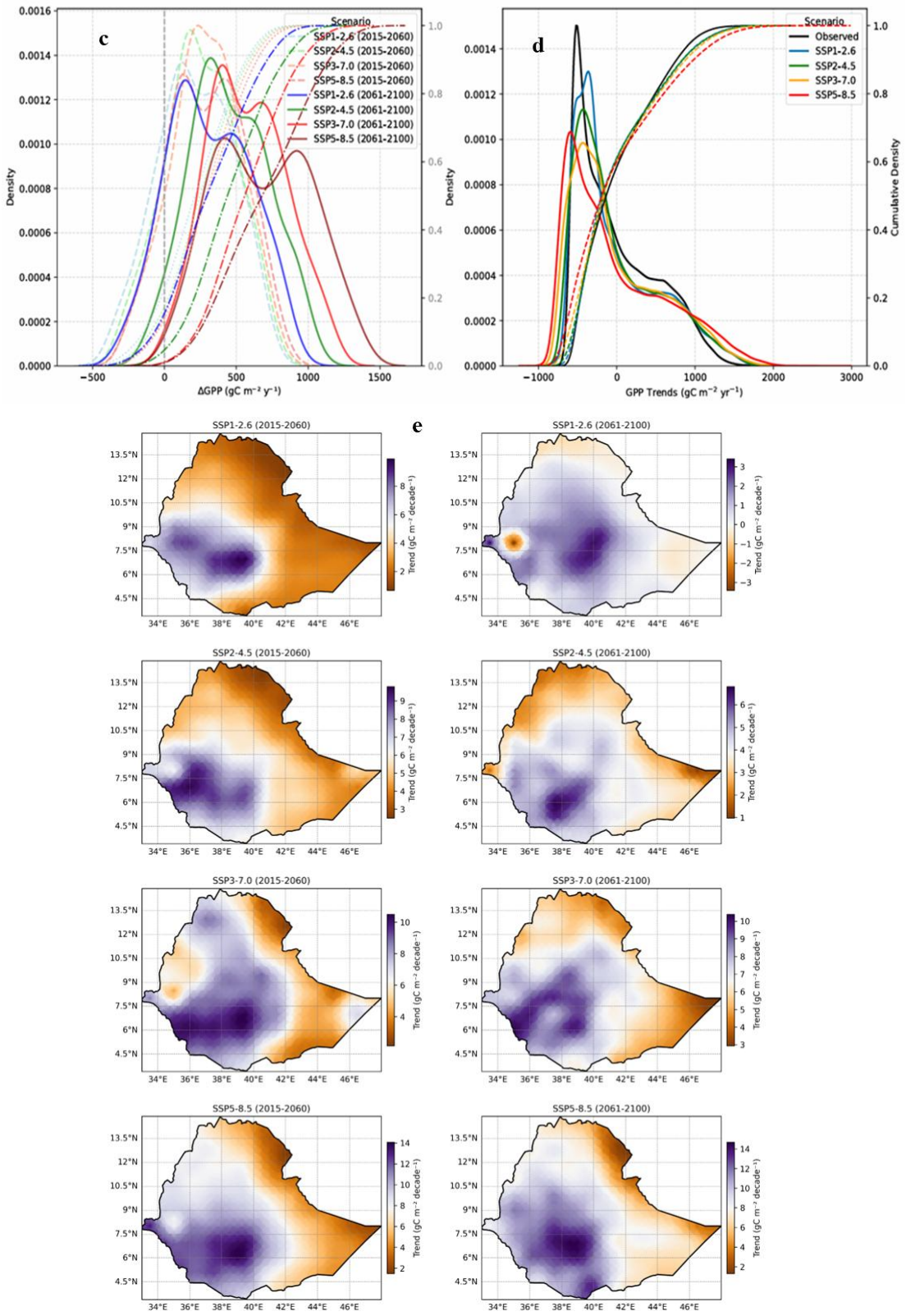

Figure 7. *(a, b) Spatiotemporal annual GPP trend with mean, standard deviation, and inter quantile range represented by box plot. (c, d) Cumulative density distribution of change in GPP and trends. (e) Spatial distribution of trend, over Ethiopia in the near 2060 (2015-2060) and far future 2100 (2061-2100) period based on six ESMs in under SSP1-2.6, SSP2-4.5, SSP3-7.0, SSP5-8.5 scenarios*

http://www.aloki.hu ● ISSN 1589 1623 (Print) ● ISSN 1785 0037 (Online)
DOI: http://dx.doi.org/10.15666/aeer/2402_31173147

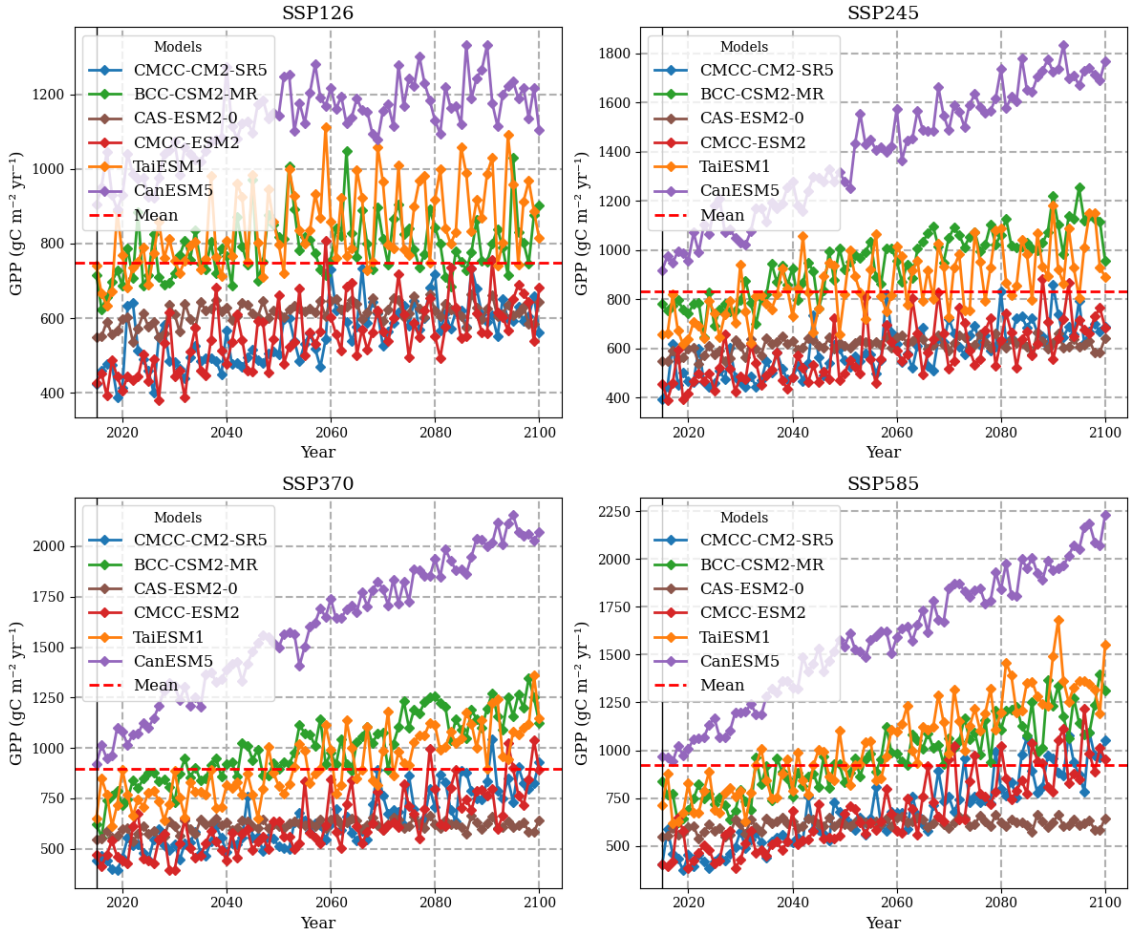

Figure 8. *Simulated GPP multimodal ensembles mean (MEM) of ESMs models from 2015-2100 in survey region*

The current and future spatial and temporal changes can be seen in the elevation gradient (slope: s) and correlation (Corr: r) between GPP and climate parameters over latitudinal variation (*Figs. 9* and *A6*, respectively). In the southern to southwestern region from 6°N to 10°N, the GPP response to temperature increased slightly from -0.13 to 0.2 g C m^{-2} yr^{-1}/°C; however, in the southwestern to northwestern region from 10°N to 12°N, it declined from 0.2 to -0.13 g C m^{-2} yr^{-1}/°C (*Fig. 9a*). In contrast, the latitude difference shows a consistent gradient in precipitation (*Fig. 9b*). There was a strong positive association between GPP and precipitation ($r = 0.4$ *to* 0.6) (*Fig. 9d*). and a fickle relationship between temperature and GPP ($r = -0.18$ *to* 0.2) (*Fig. 9c*). The spatial correlation and slopes between GPP versus temperature (-0.80 to 64, $p < 0.05$) and GPP versus precipitation (-0.3 to 0.75, $p < 0.05$) under significant *p*-value were presented (*Fig. 9e, f, g, h*).

The projected GPP from 2015 to 2100 under the SSPs climate scenario in Ethiopia varies across latitudinal differences; the mid-latitude regions (7-11°N) resulted in higher GPP in all scenarios compared to the low-latitude (3-7°N) and high-latitude (11-15°N) regions. The density distribution of yearly GPP in the mid-latitudinal regions ranges from 600 g C m^{-2} yr^{-1} to 1600 g C m^{-2} yr^{-1}, with maximum of around 900 g C m^{-2} yr^{-1} (*Fig. 10b*). Whereas lower and high latitudinal regions yearly distributions of GPP range from 400 g C m^{-2} yr^{-1} to 1400 g C m^{-2} yr^{-1} and 400 g C m^{-2} yr^{-1} to 900 g C m^{-2} yr^{-1} respectively (*Fig. 10a, c*).

http://www.aloki.hu ● ISSN 1589 1623 (Print) ● ISSN 1785 0037 (Online)
DOI: http://dx.doi.org/10.15666/aeer/2402_31173147

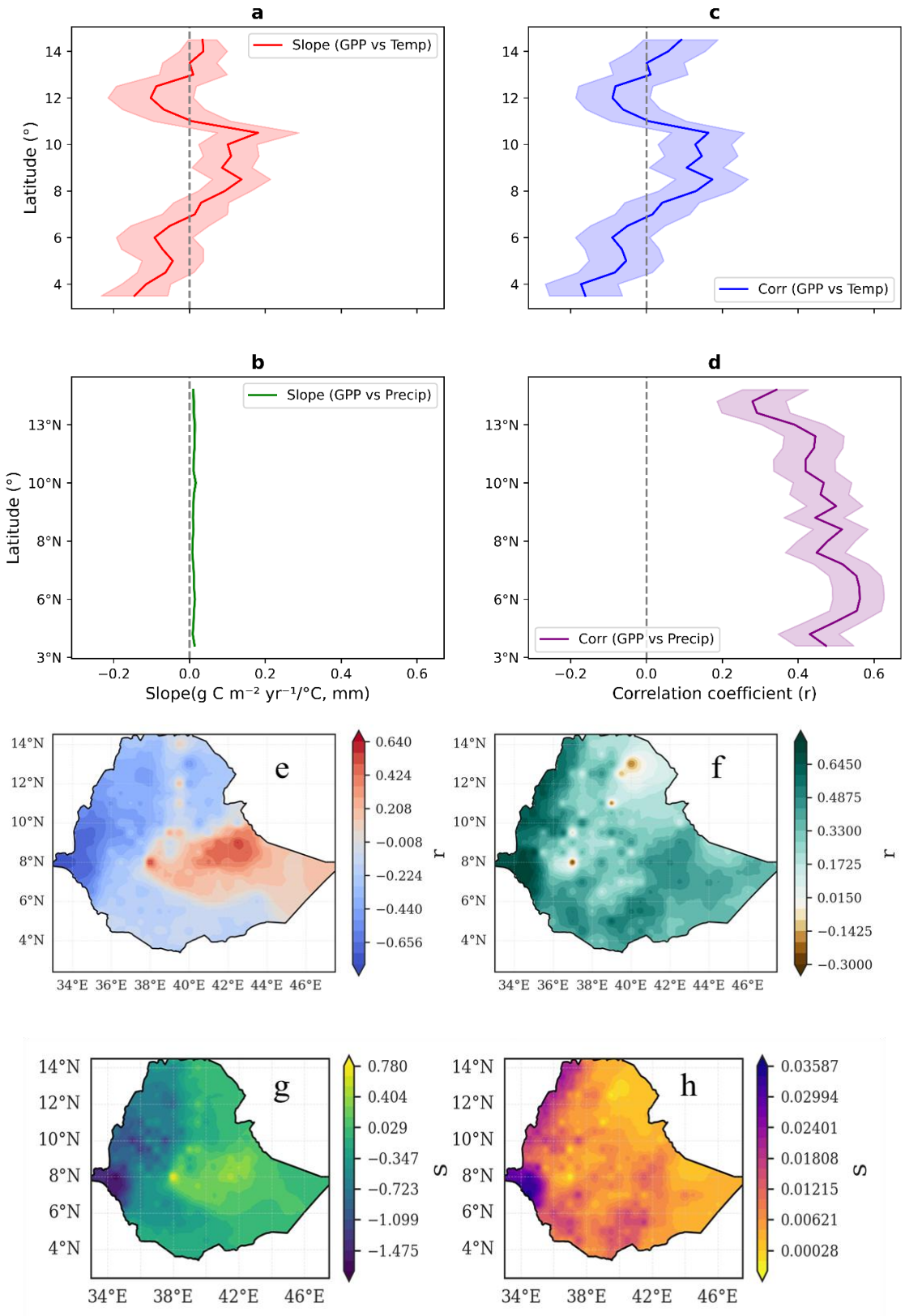

Figure 9. *Mean with 95% CI latitudinal distribution of (a) GPP-Temperature, (b) GPP-Precipitation slopes and (c) GPP-Temperature, (d) GPP- Precipitation correlations, and spatial distribution of (e) GPP-Temperature, (f) GPP- Precipitation correlation and (g) GPP-Temperature, (h) GPP- Precipitation slope in study area*

http://www.aloki.hu ● ISSN 1589 1623 (Print) ● ISSN 1785 0037 (Online)
DOI: http://dx.doi.org/10.15666/aeer/2402_31173147

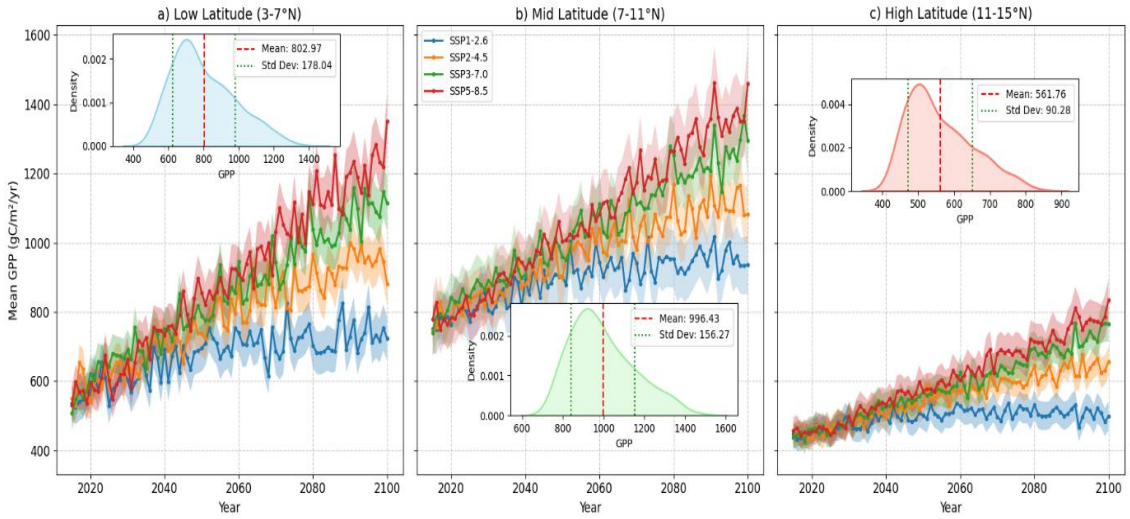

Figure 10. *Latitudinal variations of projected GPP from 2015 to 2100 under four SSPs scenario with density distribution across Ethiopia*

Discussion

The projected global warming will induce changes in terrestrial GPP in tropical regions. Ethiopia is a tropical country vulnerable to climate change. Examining the current and future spatiotemporal variation and trend of GPP in Ethiopia is significant because of climate variability and anthropogenic factors (Harris et al., 2023; Wassie, 2020). Understanding and monitoring driving factors that influence vegetation productivity in the global carbon cycle is paramount important to identify future climate change mitigation options (Cao et al., 2023; Chai and Hu, 2024; Xu et al., 2023). However, the trends of future GPP changes in this region under projected climate scenarios remain uncertain. In this study, we assessed the spatiotemporal variation and prediction of the mean annual GPP.

The spatiotemporal dynamics of historical and simulated GPP from 1982 to 2014 using the LSTM model in the highlands of Ethiopia showed significant differences based on latitude and longitude variation. GPP variation is mainly driven by climate variables, precipitation, and temperature, which govern vegetation productivity. Peak GPP values were distributed in the mid-latitude southwest region (Zhang et al., 2024a) because higher-latitude areas exhibit high temperatures and lower precipitation. The spatial distribution of GPP was more closely correlated with precipitation variation (Li et al., 2023). The findings of our study are aligned with previous research "Comparison between remote sensing and a dynamic vegetation model for estimating terrestrial primary production in Africa" (Ardö, 2015). Studies have (Xuan and Rao, 2023) revealed that precipitation is strongly correlated with the GPP. The lower elevation areas with high temperatures associated with lower precipitation results in diminishing GPP in the high emission scenarios, and our findings aligned with previous literature (Song et al., 2024; Zhu et al., 2024). The decadal growth proportions of GPP by the end of current century (2100) were to be $12.34\% \pm 8.01\%$, $36.71\% \pm 15.79\%$, $65.48\% \pm 21.61\%$, and $89.79\% \pm 27.28\%$ under SSP1-2.6, SSP2-4.5, SSP3-7.0, and SSP5-8.5 scenarios, respectively. The SSP5-8.5 scenario showed a significantly increasing trend compared to other scenarios. This research findings are consistent with the projection of NPP by CMIP6 ESMs (Varney et al., 2023). We observed the increased GPP trend in

http://www.aloki.hu ● ISSN 1589 1623 (Print) ● ISSN 1785 0037 (Online)
DOI: http://dx.doi.org/10.15666/aeer/2402_31173147

southwestern mid-latitude regions and decrease in the northeast region. The global average temperature based on the Paris Agreement proposal (Gao et al., 2017; McCulloch et al., 2024; Rogelj et al., 2016) will rise to 2°C (McKay et al., 2022) by the end of the 21st century and is likely to exceed < 5%, 32%, 80%, and 99% in Ethiopia under future SSP1-2.6, SSP2-4.5, SSP3-7.0, and SSP5-8.5, respectively. The result of the study highlights projected temperature in East Africa increased in 21st century (Umwali et al., 2025). Similarly, the change in precipitation trend per decade from 2015 to 2100 is expected to rise by 14.07 ± 71.58 mm, 12.54 ± 84.12 mm, 19.84 ± 105.69 mm, 26.48 ± 129.66 mm under SSP1-2.6, SSP2-4.5, SSP3-7.0, SSP5-8.5 scenario, respectively. Our study is coherent with Northeastern Africa precipitation projection (Taguela et al., 2025). Optimally increasing future climate variables are positively correlated with the projected GPP and total carbon storage at the end of the 21st century, which is coherent with a study conducted (Doherty et al., 2010) in East Africa. Our results are consistent with those of a study (Bogale et al., 2024) conducted (Xu et al., 2023) in East Africa, which found that temperature had a negative impact on GPP growth and precipitation had a very favorable association.

The average projected GPP during the near-future period (2015–2060) is lower than that in the far-future period (2061–2100), indicating a delayed and nonlinear response of ecosystem productivity to future climatic and atmospheric changes. A plausible explanation for this pattern is the relatively weaker CO_2 fertilization effect in the near future, particularly under medium-emission scenarios and mitigation pathways, where atmospheric CO_2 concentrations increase more gradually (Intergovernmental Panel on Climate Change (IPCC), 2023). Under such conditions, plant carbon assimilation may remain constrained, resulting in comparatively lower photosynthetic rates and GPP. In contrast, far-future projections—especially under higher-emission scenarios—are characterized by substantially elevated atmospheric CO_2 concentrations, which can enhance photosynthesis and water-use efficiency, thereby increasing terrestrial primary productivity (Walker et al., 2021; Zhu et al., 2016). This interpretation is consistent with previous studies demonstrating that CO_2 fertilization effects on vegetation productivity tend to intensify over longer timescales, although their magnitude may be moderated by nutrient limitations, climate extremes (Zhou et al., 2019), and ecosystem-specific physiological constraints (Bulut et al., 2019; Intergovernmental Panel on Climate Change (IPCC), 2023; Keenan et al., 2016). Therefore, the higher GPP projected in the far future reflects the combined influence of increased CO_2 availability and long-term ecosystem adjustment, rather than a linear or monotonic response over time.

This study explored the GPP variation in Ethiopia using a deep learning-based LSTM approach, incorporating climatic variables. While the study offers significant advantages in exploring the spatiotemporal pattern of climatic scenarios, several limitations must be acknowledged. The analysis relies on the data from 1982–2014, which represents the longest temporally consistent dataset available for Ethiopia, where long-term recent records remain limited. While the projections extend beyond the observation period, they are intended to examine long-term sensitivity of primary productivity to meteorological drivers rather than near-term prediction. Recent studies employing similar historical baselines support the continued relevance of such approaches within this data range (Agarwal et al., 2023; Elabd et al., 2025; Guo et al., 2024; Liu et al., 2024). Nevertheless, integrating updated datasets and reanalysis products in future work would help reduce uncertainty and improve projection robustness. The LSTM offers the better computing reliability of complex data but there

http://www.aloki.hu ● ISSN 1589 1623 (Print) ● ISSN 1785 0037 (Online)
DOI: http://dx.doi.org/10.15666/aeer/2402_31173147

are potential issues in data quality such as limited availability of identical high-resolution ground-truth data for validation, and the model's dependency on the quality and range of input climatic variables, which may influence our result. The accuracy of the projected GPP from the multi-model ensemble datasets using the LSTM model under future climate scenarios is uncertain (Agarwal et al., 2023; Schlund et al., 2020; Wang et al., 2024b). For LSTM model training, we used precipitation and temperature ensemble arithmetic means of ESMs datasets as model input variables, and GPP as a model output variable. The integration of multiple bias correction methods and model input variables will increase model training accuracy and GPP prediction accuracy under different future climate change scenarios. Modeling future GPP in the twenty-first century under various climate change scenarios requires the use of different machine learning model analysis techniques. We redirect future research to project vegetation productivity by considering several factors, including vegetation cover type, climate and topographic factors, CO2 concentration, population dynamics, and aerosol optical depth of tiny black carbon particles suspended in the atmosphere, to provide accurate projection and a mitigation strategy plan.

Conclusion

The LSTM model is a robust algorithm for training future climate change influences on the carbon uptake of plants using different climate factors. This study examined the GPP changes in a tropical country Ethiopia using a deep learning-based LSTM approach under future climate change scenarios. In this study, we fitted the model with the historical (1982 to 2014) GPP, and climatic data then projected the GPP using climatic variables derived from MEM of six ESMs under CMIP6 SSP1-2.6, SSP2-4.5, SSP3-7.0, SSP5-8.5 scenarios. We observed the projected climate change elevates GPP under high-emission scenarios (SSP 5-8.5, SSP 1-2.6, and SSP 2-4.5) from the near future to the far future in Ethiopia. The increasing trend in GPP values was associated with variations in geographic location and climatic factors, the lowland and arid regions exhibited consistently lower GPP. The integration of deep learning model with climatic scenarios in tropical zone of this study comprehensively investigate the dynamics of GPP. As far as the authors are aware, this is one of the first attempts to use this method for estimating GPP in Ethiopia's tropical regions. By shedding light on these dynamics, this study aimed to bolster conservation measures and underscore the urgent need to address the influence of projected climate change on GPP. The findings of this study serve as a crucial reference for policymakers, ecologists, and other stakeholders, urging them to recognize the effects of future warming and prioritize initiative-taking mitigation efforts to achieve climate-resilient green economy strategies with net zero CO_2 emissions of SDG 2030 agenda.

Funding. This research was supported by Basic Science Research Program through the National Research Foundation of Korea (NRF) funded by the Ministry of Education (RS2022NR071158) Republic of Korea.

Conflict of interests. The authors declare that they have no known competing monetary interests or personal relationships that could have influenced the work reported in this study.

Data availability. The Coupled Model Intercomparison Project (CMIP6) simulated historical and future GPP dataset accessed from six Earth System Models (ESMs) with the same variant label r1i1p1f1 stands ('*r'* realization, 'i*'* initialization, '*p'* physics, '*f'* forcing), monthly and grid label "gn", which is available an online archive (https://esgf-node.ornl.gov/search) used to reduce differences among six ESMs under four future

http://www.aloki.hu ● ISSN 1589 1623 (Print) ● ISSN 1785 0037 (Online)
DOI: http://dx.doi.org/10.15666/aeer/2402_31173147

climate scenario (SSP1-2.6, SSP2-4.5, SSP3-7.0, SSP5-8.5). Monthly climate datasets (precipitation and temperature) were extracted from the Climate Research Unit Time Series version 4.00 (CRU TS v4.00) from 1901 to 2015 at a 0.5° × 0.5° grid resolution from the UK National Center for Atmospheric Science (https://doi.org/10.1029/2022EF003395). Monthly GPP was extracted from an improved light-use efficiency model (https://daac.ornl.gov/cgi-bin/dsviewer.pl?ds_id=1789). The Digital Elevation Model (DEM) was obtained from the global DEM dataset with a NOAA spatial resolution of 1 km (https://www.ncei.noaa.gov/products/etopo-global-relief-model) (https://doi.org/10.1029/2023EF003903).

REFERENCES

[1] Agarwal, G., Deb Burman, P. K., Kulkarni, V. Y., Kosamkar, P. K. (2023): Prediction of gross primary productivity using hybrid LSTM-GRU neural networks and ERA5-reanalysis data. – Proceedings - 4th IEEE 2023 International Conference on Computing, Communication, and Intelligent Systems, ICCCIS 2023, pp. 94-99.

[2] Al Mehedi, M. A., Amur, A., Metcalf, J., McGauley, M., Smith, V., Wadzuk, B. (2023): Predicting the performance of green stormwater infrastructure using multivariate long short-term memory (LSTM) neural network. – Journal of Hydrology 625: 130076.

[3] Alkama, R., Forzieri, G., Duveiller, G., Grassi, G., Liang, S., Cescatti, A. (2022): Vegetation-based climate mitigation in a warmer and greener World. – Nature Communications 13(1): 1-10.

[4] Allen, B. J., Hill, D. J., Burke, A. M., Clark, M., Marchant, R., Stringer, L. C., Williams, D. R., Lyon, C. (2024): Projected future climatic forcing on the global distribution of vegetation types. – Philosophical Transactions of the Royal Society B 379(1902):

[5] Almazroui, M., Saeed, F., Saeed, S., Nazrul Islam, M., Ismail, M., Klutse, N. A. B., Siddiqui, M. H. (2020): Projected change in temperature and precipitation over Africa from CMIP6. – Earth Systems and Environment 4(3): 455-475.

[6] Almazroui, M., Islam, M. N., Saeed, F., Saeed, S., Ismail, M., Ehsan, M. A., Diallo, I., O'Brien, E., Ashfaq, M., Martínez-Castro, D., Cavazos, T., Cerezo-Mota, R., Tippett, M. K., Gutowski, W. J., Alfaro, E. J., Hidalgo, H. G., Vichot-Llano, A., Campbell, J. D., Kamil, S., et al. (2021a): Projected changes in temperature and precipitation over the United States, Central America, and the Caribbean in CMIP6 GCMs. – Earth Systems and Environment 5(1): 1-24.

[7] Almazroui, M., Ashfaq, M., Islam, M. N., Rashid, I. U., Kamil, S., Abid, M. A., O'Brien, E., Ismail, M., Reboita, M. S., Sörensson, A. A., Arias, P. A., Alves, L. M., Tippett, M. K., Saeed, S., Haarsma, R., Doblas-Reyes, F. J., Saeed, F., Kucharski, F., Nadeem, I., et al. (2021b): Assessment of CMIP6 Performance and projected temperature and precipitation changes over South America. – Earth Systems and Environment 5(2): 155-183.

[8] Anav, A., Friedlingstein, P., Kidston, M., Bopp, L., Ciais, P., Cox, P., Jones, C., Jung, M., Myneni, R., Zhu, Z. (2013): Evaluating the land and ocean components of the global carbon cycle in the CMIP5 earth system models. – Journal of Climate 26(18): 6801-6843.

[9] Anav, A., Friedlingstein, P., Beer, C., Ciais, P., Harper, A., Jones, C., Murray-Tortarolo, G., Papale, D., Parazoo, N. C., Peylin, P., Piao, S., Sitch, S., Viovy, N., Wiltshire, A., Zhao, M. (2015): Spatiotemporal patterns of terrestrial gross primary production: a review. – Reviews of Geophysics 53(3): 785-818.

[10] Ardö, J. (2015): Comparison between remote sensing and a dynamic vegetation model for estimating terrestrial primary production of Africa. – Carbon Balance and Management 10(1): 1-15.

[11] Assfaw, M. T., Neka, B. G., Ayele, E. G. (2023): Modeling the impact of climate change on streamflow responses in the Kessem watershed, Middle Awash sub-basin, Ethiopia. – Journal of Water and Climate Change 14(12): 4837-4859.

[12] Azad, N., Ahmadi, A. (2024): Assessment of CMIP6 models and multi-model averaging for temperature and precipitation over Iran. – Scientific Reports 14(1): 1-19.

http://www.aloki.hu ● ISSN 1589 1623 (Print) ● ISSN 1785 0037 (Online)
DOI: http://dx.doi.org/10.15666/aeer/2402_31173147

[13] Bai, Y., Liang, S., Jia, A., Li, S. (2023): different satellite products revealing variable trends in global gross primary production. – Journal of Geophysical Research: Biogeosciences 128(7): e2022JG006918.
[14] Berhanu, D., Alamirew, T., Bewket, W., Tarkegn, T. G., Zeleke, G., Haileslassie, A., O'Donnell, G., Walsh, C. L., Gebrehiwot, S. (2025): Evaluation of CMIP6 models in simulating seasonal extreme precipitation over Ethiopia. – Weather and Climate Extremes 47: 100752.
[15] Berihun, M. L., Tsunekawa, A., Haregeweyn, N., Tsubo, M., Yasuda, H., Fenta, A. A., Dile, Y. T., Bayabil, H. K., Tilahun, S. A. (2023): Examining the past 120 years' climate dynamics of Ethiopia. – Theoretical and Applied Climatology 154(1-2): 535-566.
[16] Bi, W., He, W., Zhou, Y., Ju, W., Liu, Y., Liu, Y., Zhang, X., Wei, X., Cheng, N. (2022): A global 0.05° dataset for gross primary production of sunlit and shaded vegetation canopies from 1992 to 2020. – Scientific Data 9(1): 1-13.
[17] Bogale, T., Degefa, S., Dalle, G., Abebe, G. (2024): Spatiotemporal dynamics of vegetation net primary productivity and its response to climate variability. – Environmental Systems Research 13(1): 1-13.
[18] Bongasie, A., Dhakal, T., Ayalew, A., Kim, T. S., Lee, Y., Jang, G. S. (2024): Analysis of forest cover change and its driving factors in Senan district, Amhara Region, Ethiopia. – Environmental Monitoring and Assessment 196(4).
[19] Bulut, S., Satir, O., Günlü, A. (2019): Determining the interactions of black pine net primary productivity and forest stand parameters in northern Turkey. – Applied Ecology and Environmental Research 17(2): 4459-4473.
[20] Cannon, A. J., Sobie, S. R., Murdock, T. Q. (2015): Bias correction of GCM precipitation by quantile mapping: How well do methods preserve changes in quantiles and extremes? Journal of Climate 28(17): 6938-6959.
[21] Cao, D., Zhang, J., Xun, L., Yang, S., Wang, J., Yao, F. (2021): Spatiotemporal variations of global terrestrial vegetation climate potential productivity under climate change. – Science of the Total Environment 770: 145320.
[22] Cao, D., Zhang, J., Zhang, T., Yao, F., Ji, R., Zi, S., Li, H., Cheng, Q. Y. (2023): Spatiotemporal variations and driving factors of global terrestrial vegetation productivity gap under the changing of climate, CO2, landcover and N deposition. – Science of the Total Environment 880.
[23] Chai, Y., Hu, Y. (2024): Characteristics and drivers of vegetation productivity sensitivity to increasing CO2 at northern middle and high latitudes. – Ecology and Evolution 14(5): e11467.
[24] Chen, J. M. (2021): Carbon neutrality: toward a sustainable future. – The Innovation 2(3): 100127.
[25] Chen, Z., Liu, H., Xu, C., Wu, X., Liang, B., Cao, J., Chen, D. (2021): Modeling vegetation greenness and its climate sensitivity with deep-learning technology. – Ecology and Evolution 11(12): 7335-7345.
[26] Chen, Z. T., Liu, H. Y., Xu, C. Y., Wu, X. C., Liang, B. Y., Cao, J., Chen, D. (2022): Deep learning projects future warming-induced vegetation growth changes under SSP scenarios. – Advances in Climate Change Research 13(2): 251-257.
[27] Chin, S., Lloyd, V. (2024): Predicting climate change using an autoregressive long short-term memory model. – Frontiers in Environmental Science 12: 1301343.
[28] Climate Action Tracker (2020): Climate Governance in Ethiopia.
[29] Dagne, A., Corfee-Morlot, J., Elliott, C., Bassi, A. M., Pallaske, G., Payosova, I., Pellerin, M., Guzzetti, M. (2023): Ethiopia's path to net zero and climate-resilient development: policies, costs, and co-benefits. – World Resources Institute.
[30] DeAngelo, J., Azevedo, I., Bistline, J., Clarke, L., Luderer, G., Byers, E., Davis, S. J. (2021): Energy systems in scenarios at net-zero CO2 emissions. – Nature Communications 12(1): 1-10.

http://www.aloki.hu ● ISSN 1589 1623 (Print) ● ISSN 1785 0037 (Online)
DOI: http://dx.doi.org/10.15666/aeer/2402_31173147

[31] Doherty, R. M., Sitch, S., Smith, B., Lewis, S. L., Thornton, P. K. (2010): Implications of future climate and atmospheric CO2 content for regional biogeochemistry, biogeography and ecosystem services across East Africa. – Global Change Biology 16(2): 617-640.
[32] Elabd, E., Hamouda, H. M., Ali, M. A. M., Fouad, Y. (2025): Climate change prediction in Saudi Arabia using a CNN GRU LSTM hybrid deep learning model in al Qassim region. – Scientific Reports 15(1): 16275.
[33] Enyew, F. B., Sahlu, D., Tarekegn, G. B., Hama, S., Debele, S. E. (2024): Performance evaluation of CMIP6 Climate model projections for precipitation and temperature in the Upper Blue Nile Basin, Ethiopia. – Climate 12(11).
[34] Eyring, V., Bony, S., Meehl, G. A., Senior, C. A., Stevens, B., Stouffer, R. J., Taylor, K. E. (2016): Overview of the Coupled Model Intercomparison Project Phase 6 (CMIP6) experimental design and organization. – Geoscientific Model Development 9(5): 1937-1958.
[35] Fan, X., Duan, Q., Shen, C., Wu, Y., Xing, C. (2020): Global surface air temperatures in CMIP6: historical performance and future changes. – Environmental Research Letters 15(10): 104056.
[36] Fang, Z., Zhang, W., Wang, L., Schurgers, G., Ciais, P., Peñuelas, J., Brandt, M., Yang, H., Huang, K., Shen, Q., Rasmus, F. (2024): Global increase in the optimal temperature for the productivity of terrestrial ecosystems. – Communications Earth & Environment 5(1): 1-9.
[37] Fauzi, F., Kuswanto, H., Atok, R. M. (2020): Bias correction and statistical downscaling of earth system models using quantile delta mapping (QDM) and bias correction constructed analogues with quantile mapping recording (BCCAQ). – Journal of Physics: Conference Series 1538(1): 012050.
[38] Firpo, M. Â. F., Guimarães, B. dos S., Dantas, L. G., Silva, M. G. B. da, Alves, L. M., Chadwick, R., Llopart, M. P., Oliveira, G. S. de. (2022): Assessment of CMIP6 models' performance in simulating present-day climate in Brazil. – Frontiers in Climate 4: 948499.
[39] Gao, Y., Gao, X., Zhang, X. (2017): The 2 °C global temperature target and the evolution of the long-term goal of addressing climate change—from the United Nations Framework Convention on Climate Change to the Paris Agreement. – Engineering 3(2): 272-278.
[40] Gergel, D. R., Malevich, S. B., McCusker, K. E., Tenezakis, E., Delgado, M. T., Fish, M. A., Kopp, R. E. (2024): Global Downscaled Projections for Climate Impacts Research (GDPCIR): preserving quantile trends for modeling future climate impacts. – Geoscientific Model Development 17(1): 191-227.
[41] Getachew Mengistu, A., Mengistu Tsidu, G., Koren, G., Kooreman, M. L., Folkert Boersma, K., Tagesson, T., Ardö, J., Nouvellon, Y., Peters, W. (2021): Sun-induced fluorescence and near-infrared reflectance of vegetation track the seasonal dynamics of gross primary production over Africa. – Biogeosciences 18(9): 2843-2857.
[42] Getnet, G. T., Dagnew, A. B., Ayal, D. Y. (2023): Spatiotemporal variability and trends of rainfall and temperature in the tropical moist montane ecosystem: implications to climate-smart agriculture in Geshy watershed, Southwest Ethiopia. – Climate Services 30: 100384.
[43] Ghazi, B., Salehi, H., Przybylak, R., Pospieszyńska, A. (2025): Projection of climate change impact on the occurrence of drought events in Poland. – Scientific Reports 15(1): 1-14.
[44] Gidden, M. J., Riahi, K., Smith, S. J., Fujimori, S., Luderer, G., Kriegler, E., Van Vuuren, D. P., Van Den Berg, M., Feng, L., Klein, D., Calvin, K., Doelman, J. C., Frank, S., Fricko, O., Harmsen, M., Hasegawa, T., Havlik, P., Hilaire, J., Hoesly, R., et al. (2019): Global emissions pathways under different socioeconomic scenarios for use in CMIP6: a dataset of harmonized emissions trajectories through the end of the century. – Geoscientific Model Development 12(4): 1443-1475.
[45] Gottfried, M., Pauli, H., Futschik, A., Akhalkatsi, M., Barančok, P., Benito Alonso, J. L., Coldea, G., Dick, J., Erschbamer, B., Fernández Calzado, M. R., Kazakis, G., Krajči, J., Larsson, P., Mallaun, M., Michelsen, O., Moiseev, D., Moiseev, P., Molau, U., Merzouki,

http://www.aloki.hu ● ISSN 1589 1623 (Print) ● ISSN 1785 0037 (Online)
DOI: http://dx.doi.org/10.15666/aeer/2402_31173147

A., et al. (2012): Continent-wide response of mountain vegetation to climate change. – Nature Climate Change 2(2): 111-115.
[46] Graves, A. (2013): Generating sequences with recurrent neural networks. – arXiv.
[47] Guo, E., Wang, Y., Wang, C., Sun, Z., Bao, Y., Mandula, N., Jirigala, B., Bao, Y., Li, H. (2021): NDVI indicates long-term dynamics of vegetation and its driving forces from climatic and anthropogenic factors in Mongolian Plateau. – Remote Sensing 13(4).
[48] Guo, H., Zhou, X., Dong, Y., Wang, Y., Li, S. (2023): On the use of machine learning methods to improve the estimation of gross primary productivity of maize field with drip irrigation. – Ecological Modelling 476: 110250.
[49] Guo, Q., He, Z., Wang, Z. (2024): Monthly climate prediction using deep convolutional neural network and long short-term memory. – Scientific Reports 14(1): 1-17.
[50] Harris, I., Osborn, T. J., Jones, P., Lister, D. (2020): Version 4 of the CRU TS monthly high-resolution gridded multivariate climate dataset. – Scientific Data 7(1): 1-18.
[51] Harris, L. B., Taylor, A. H., Kassa, H., Leta, S., Powell, B. (2023): Humans and climate modulate fire activity across Ethiopia. – Fire Ecology 19(1): 1-16.
[52] He, B., Chen, A., Wang, H., Wang, Q. (2015): Dynamic response of satellite-derived vegetation growth to climate change in the three north shelter forest region in China. – Remote Sensing 7(8).
[53] Hochreiter, S., Schmidhuber, J. (1997): Long short-term memory. – Neural Computation 9(8): 1735-1780.
[54] Intergovernmental Panel on Climate Change (IPCC) (2023): Climate Change 2021—The Physical Science Basis. – Cambridge University Press, Cambridge.
[55] Jacob, D., Teichmann, C., Sobolowski, S., Katragkou, E., Anders, I., Belda, M., Benestad, R., Boberg, F., Buonomo, E., Cardoso, R. M., Casanueva, A., Christensen, O. B., Christensen, J. H., Coppola, E., De Cruz, L., Davin, E. L., Dobler, A., Domínguez, M., Fealy, R., et al. (2020): Regional climate downscaling over Europe: perspectives from the EURO-CORDEX community. – Regional Environmental Change 20(2): 1-20.
[56] Kayiranga, A., Chen, B., Wang, F., Nthangeni, W., Dilawar, A., Hategekimana, Y., Zhang, H., Guo, L. (2022): Spatiotemporal variation in gross primary productivity and their responses to climate in the Great Lakes Region of Sub-Saharan Africa during 2001-2020. – Sustainability 14(5): 2610.
[57] Keenan, T. F., Prentice, I. C., Canadell, J. G., Williams, C. A., Wang, H., Raupach, M., Collatz, G. J. (2016): Recent pause in the growth rate of atmospheric CO2 due to enhanced terrestrial carbon uptake. – Nature Communications 7.
[58] Khalifa, M., Elagib, N. A., Ribbe, L., Schneider, K. (2018): Spatio-temporal variations in climate, primary productivity and efficiency of water and carbon use of the land cover types in Sudan and Ethiopia. – Science of the Total Environment 624: 790-806.
[59] Kong, R., Zhang, Z., Huang, R., Tian, J., Feng, R., Chen, X. (2022): Projected global warming-induced terrestrial ecosystem carbon across China under SSP scenarios. – Ecological Indicators 139: 108963.
[60] Lecun, Y., Bengio, Y., Hinton, G. (2015): Deep learning. – Nature 521(7553): 436-444.
[61] Li, G., Chen, W., Mu, L., Zhang, X., Bi, P., Wang, Z., Yang, Z. (2023): Analysis and prediction of global vegetation dynamics: past variations and future perspectives. – Journal of Forestry Research 34(2): 317-332.
[62] Li, L., Zha, Y., Zhang, J., Li, Y., Lyu, H. (2020): Effect of terrestrial vegetation growth on climate change in China. – Journal of Environmental Management 262: 110321.
[63] Li, M., Zhu, Z., Ren, W., Wang, Y. (2024): Predicting gross primary productivity under future climate change for the Tibetan Plateau based on convolutional neural networks. – Remote Sensing 16(19): 3723.
[64] Li, W. P., Zhang, Y. W., Mu, M., Shi, X. L., Zhou, W. Y., Ji, J. J. (2023): Spatial and temporal variations of gross primary production simulated by land surface model BCC_AVIM2.0. – Advances in Climate Change Research 14(2): 286-299.

http://www.aloki.hu ● ISSN 1589 1623 (Print) ● ISSN 1785 0037 (Online)
DOI: http://dx.doi.org/10.15666/aeer/2402_31173147

[65] Liu, L., Zhou, W., Guan, K., Peng, B., Xu, S., Tang, J., Zhu, Q., Till, J., Jia, X., Jiang, C., Wang, S., Qin, Z., Kong, H., Grant, R., Mezbahuddin, S., Kumar, V., Jin, Z. (2024): Knowledge-guided machine learning can improve carbon cycle quantification in agroecosystems. – Nature Communications 15(1): 357.
[66] Lomax, G. A., Powell, T. W. R., Lenton, T. M., Economou, T., Cunliffe, A. M. (2024): Untangling the environmental drivers of gross primary productivity in African rangelands. – Communications Earth & Environment 5(1): 500.
[67] Lu, J., Wang, G., Feng, D., Nooni, I. K. (2023): Improving the gross primary production estimate by merging and downscaling based on deep learning. – Forests 14(6): 1201.
[68] Lu, Q., Liu, H., Wei, L., Zhong, Y., Zhou, Z. (2024): Global prediction of gross primary productivity under future climate change. – Science of the Total Environment 912: 169239.
[69] Luhunga, P. M. (2025): Projected changes in climate extremes over Tanzania. – Scientific Reports 15(1): 1-15.
[70] Ma, Y., Hu, Y., Moncrieff, G. R., Slingsby, J. A., Wilson, A. M., Maitner, B., Zhenqi Zhou, R. (2022): Forecasting vegetation dynamics in an open ecosystem by integrating deep learning and environmental variables. – International Journal of Applied Earth Observation and Geoinformation 114: 103060.
[71] Makula, E. K., Zhou, B. (2022): Coupled Model Intercomparison Project phase 6 evaluation and projection of East African precipitation. – International Journal of Climatology 42(4): 2398-2412.
[72] Martinuzzi, F., Mahecha, M. D., Camps-Valls, G., Montero, D., Williams, T., Mora, K. (2024): Learning extreme vegetation response to climate drivers with recurrent neural networks. – Nonlinear Processes in Geophysics 31(4): 535-557.
[73] McCulloch, M. T., Winter, A., Sherman, C. E., Trotter, J. A. (2024): 300 years of sclerosponge thermometry shows global warming has exceeded 1.5 °C. – Nature Climate Change 14(2): 171-177.
[74] McKay, D. I. A., Staal, A., Abrams, J. F., Winkelmann, R., Sakschewski, B., Loriani, S., Fetzer, I., Cornell, S. E., Rockström, J., Lenton, T. M. (2022): Exceeding 1.5°C global warming could trigger multiple climate tipping points. – Science 377(6611).
[75] Meinshausen, M., Nicholls, Z. R. J., Lewis, J., Gidden, M. J., Vogel, E., Freund, M., Beyerle, U., Gessner, C., Nauels, A., Bauer, N., Canadell, J. G., Daniel, J. S., John, A., Krummel, P. B., Luderer, G., Meinshausen, N., Montzka, S. A., Rayner, P. J., Reimann, S., et al. (2020): The shared socio-economic pathway (SSP) greenhouse gas concentrations and their extensions to 2500. – Geoscientific Model Development 13(8): 3571-3605.
[76] Montero, D., Mahecha, M. D., Martinuzzi, F., Aybar, C., Klosterhalfen, A., Knohl, A., Koebsch, F., Anaya, J., Wieneke, S. (2024): recurrent neural networks for modelling gross primary production. – 4214-4217.
[77] Nolan, C., Overpeck, J. T., Allen, J. R. M., Anderson, P. M., Betancourt, J. L., Binney, H. A., Brewer, S., Bush, M. B., Chase, B. M., Cheddadi, R., Djamali, M., Dodson, J., Edwards, M. E., Gosling, W. D., Haberle, S., Hotchkiss, S. C., Huntley, B., Ivory, S. J., Kershaw, A. P., et al. (2018): Past and future global transformation of terrestrial ecosystems under climate change. – Science 361(6405): 920-923.
[78] Ossó, A., Craig, P., Allan, R. P. (2023): An assessment of CMIP6 climate signals and biases in temperature, precipitation and soil moisture over Europe. – International Journal of Climatology 43(12): 5698-5719.
[79] Pan, S., Dangal, S. R. S., Tao, B., Yang, J., Tian, H. (2015): Recent patterns of terrestrial net primary production in Africa influenced by multiple environmental changes. – Ecosystem Health and Sustainability 1(5): 1-15.
[80] Park, H., Jeong, S. (2021): Leaf area index in Earth system models: how the key variable of vegetation seasonality works in climate projections. – Environmental Research Letters 16(3).

http://www.aloki.hu ● ISSN 1589 1623 (Print) ● ISSN 1785 0037 (Online)
DOI: http://dx.doi.org/10.15666/aeer/2402_31173147

[81] Peng, S., Wang, C., Li, Z., Mihara, K., Kuramochi, K., Toma, Y., Hatano, R. (2023): Climate change multi-model projections in CMIP6 scenarios in Central Hokkaido, Japan. – Scientific Reports 13(1): 1-18.
[82] Qian, L., Yu, X., Zhang, Z., Wu, L., Fan, J., Xiang, Y., Chen, J., Liu, X. (2024): Assessing and improving the high uncertainty of global gross primary productivity products based on deep learning under extreme climatic conditions. – Science of the Total Environment 957: 177344.
[83] Reichstein, M., Bahn, M., Ciais, P., Frank, D., Mahecha, M. D., Seneviratne, S. I., Zscheischler, J., Beer, C., Buchmann, N., Frank, D. C., Papale, D., Rammig, A., Smith, P., Thonicke, K., Van Der Velde, M., Vicca, S., Walz, A., Wattenbach, M. (2013): Climate extremes and the carbon cycle. – Nature 500(7462): 287-295.
[84] Reichstein, M., Camps-Valls, G., Stevens, B., Jung, M., Denzler, J., Carvalhais, N., Prabhat. (2019): Deep learning and process understanding for data-driven Earth system science. – Nature 566(7743): 195-204.
[85] Rettie, F. M., Gayler, S., Weber, T. K. D., Tesfaye, K., Streck, T. (2023b): High-resolution CMIP6 climate projections for Ethiopia using the gridded statistical downscaling method. – Scientific Data 10(1): 1-18.
[86] Riahi, K., van Vuuren, D. P., Kriegler, E., Edmonds, J., O'Neill, B. C., Fujimori, S., Bauer, N., Calvin, K., Dellink, R., Fricko, O., Lutz, W., Popp, A., Cuaresma, J. C., KC, S., Leimbach, M., Jiang, L., Kram, T., Rao, S., Emmerling, J., et al. (2017): The Shared Socioeconomic Pathways and their energy, land use, and greenhouse gas emissions implications: an overview. – Global Environmental Change 42: 153-168.
[87] Rogelj, J., Den Elzen, M., Höhne, N., Fransen, T., Fekete, H., Winkler, H., Schaeffer, R., Sha, F., Riahi, K., Meinshausen, M. (2016): Paris Agreement climate proposals need a boost to keep warming well below 2 °C. – Nature 534(7609): 631-639.
[88] Schlund, M., Eyring, V., Camps-Valls, G., Friedlingstein, P., Gentine, P., Reichstein, M. (2020): Constraining uncertainty in projected gross primary production with machine learning. – Journal of Geophysical Research: Biogeosciences 125(11): e2019JG005619.
[89] Shao, W., Wu, C., Yue, T., Zhao, N., Hu, Y. (2025): Prediction of gross primary productivity change in Central Asia under climate change using deep learning. – IEEE Journal of Selected Topics in Applied Earth Observations and Remote Sensing.
[90] Shi, S., Yang, P., Vrieling, A., Tol, C. van der. (2025): Vegetation optimal temperature modulates global vegetation season onset shifts in response to warming climate. – Communications Earth & Environment 6(1): 1-9.
[91] Smith, T. M., Smith, J. B., Shugart, H. H. (1992): Modeling the response of terrestrial vegetation to climate change in the tropics. – Tropical Forests in Transition 253-268.
[92] Song, J., Zhou, S., Yu, B., Li, Y., Liu, Y., Yao, Y., Wang, S., Fu, B. (2024): Serious underestimation of reduced carbon uptake due to vegetation compound droughts. – NPJ Climate and Atmospheric Science 7(1): 1-11
[93] Song, Y. H., Chung, E. S., Shahid, S. (2021): Spatiotemporal differences and uncertainties in projections of precipitation and temperature in South Korea from CMIP6 and CMIP5 general circulation models. – International Journal of Climatology 41(13): 5899-5919.
[94] Taguela, T. N., Akinsanola, A. A., Adeliyi, T. E., Rhoades, A., Nazarian, R. H. (2025): Understanding drivers and uncertainty in projected African precipitation. – NPJ Climate and Atmospheric Science 8(1): 222
[95] Tesfaye, Y., Dechassa, N., Alemayehu, Y., Birhan, D. A. (2025): Spatiotemporal variability and trends in extreme rainfall and temperature indices in Southeastern Oromia, Ethiopia. – Scientific Reports 15(1): 29782.
[96] Ugbaje, S. U., Odeh, I. O. A., Bishop, T. F. A., Li, J. (2017): Assessing the spatio-temporal variability of vegetation productivity in Africa: quantifying the relative roles of climate variability and human activities. – International Journal of Digital Earth 10(9): 879-900.
[97] Umwali, E. D., Chen, X., Ma, X., Guo, Z., Mbigi, D., Zhang, Z., Umugwaneza, A., Gasirabo, A., Umuhoza, J. (2025): Integrated SSP-RCP scenarios for modeling the impacts

http://www.aloki.hu ● ISSN 1589 1623 (Print) ● ISSN 1785 0037 (Online)
DOI: http://dx.doi.org/10.15666/aeer/2402_31173147

of climate change and land use on ecosystem services in East Africa. – Ecological Modelling 504: 111092.
[98] Varney, R. M., Chadburn, S. E., Burke, E. J., Jones, S., Wiltshire, A. J., Cox, P. M. (2023): Simulated responses of soil carbon to climate change in CMIP6 Earth system models: the role of false priming. – Biogeosciences 20(18): 3767-3790.
[99] Vasilakos, C., Tsekouras, G. E., Kavroudakis, D. (2022): LSTM-based prediction of mediterranean vegetation dynamics using NDVI time-series data. – Land 11(6): 923.
[100] Walker, A. P., De Kauwe, M. G., Bastos, A., Belmecheri, S., Georgiou, K., Keeling, R. F., McMahon, S. M., Medlyn, B. E., Moore, D. J. P., Norby, R. J., Zaehle, S., Anderson-Teixeira, K. J., Battipaglia, G., Brienen, R. J. W., Cabugao, K. G., Cailleret, M., Campbell, E., Canadell, J. G., Ciais, P., et al. (2021): Integrating the evidence for a terrestrial carbon sink caused by increasing atmospheric CO2. – The New Phytologist 229(5): 2413-2445.
[101] Wang, B., Smith, B., Waters, C., Feng, P., Liu, D. L. (2024a): Modelling changes in vegetation productivity and carbon balance under future climate scenarios in southeastern Australia. – Science of The Total Environment 924: 171748.
[102] Wang, F., Tian, D. (2022): On deep learning-based bias correction and downscaling of multiple climate models simulations. – Climate Dynamics 59(11-12): 3451-3468.
[103] Wang, F., Tian, D. (2024): Multivariate bias correction and downscaling of climate models with trend-preserving deep learning. – Climate Dynamics 62(10): 9651-9672.
[104] Wang, J., Wang, Y., Xie, X., Zhao, W., Wu, C., Guan, X., Yang, T. (2024b): Climate-induced uncertainty in modeling gross primary productivity from the light use efficiency approach. – Journal of Geophysical Research: Biogeosciences 129(10): e2024JG008394.
[105] Wang, Q., Liang, L., Wang, S., Wang, S., Zhang, L., Qiu, S., Shi, Y., Shi, J., Sun, C. (2023): Insights into spatiotemporal variations in the NPP of terrestrial vegetation in Africa from 1981 to 2018. – Remote Sensing 15(11): 2748.
[106] Wang, S., Zhang, Y., Ju, W., Qiu, B., Zhang, Z. (2021): Tracking the seasonal and inter-annual variations of global gross primary production during last four decades using satellite near-infrared reflectance data. – Science of the Total Environment 755: 142569.
[107] Wassie, S. B. (2020): Natural resource degradation tendencies in Ethiopia: a review. – Environmental Systems Research 9(1): 1-29.
[108] Wei, J., Liu, X., Zhou, B. (2023): Sensitivity of vegetation to climate in mid-to-high latitudes of asia and future vegetation projections. – Remote Sensing 15(10): 2648.
[109] Wei, J., Pu, Y., Liu, X., Shan, Y., Zhou, B. (2024): Analyzing uncertainty and constraining projections for future vegetation in mid-to-high-latitude Asia. – Atmospheric and Oceanic Science Letters 100522.
[110] Wen, Y., Liu, X., Xin, Q., Wu, J., Xu, X., Pei, F., Li, X., Du, G., Cai, Y., Lin, K., Yang, J., Wang, Y. (2019): Cumulative effects of climatic factors on terrestrial vegetation growth. – Journal of Geophysical Research: Biogeosciences 124(4): 789-806.
[111] Wu, M., Jiang, F., Scholze, M., Chen, D., Ju, W., Wang, S., Kaminski, T., Lu, Z., Vossbeck, M., Zheng, M. (2024): Regional responses of vegetation productivity to the two phases of ENSO. – Geophysical Research Letters 51(8): e2024GL108176.
[112] Xie, B., Jia, X., Qin, Z., Shen, J., Chang, Q. (2016): Vegetation dynamics and climate change on the Loess Plateau, China: 1982-2011. – Regional Environmental Change 16(6).
[113] Xiong, Z., Zhang, Z., Gui, H., Zhu, P., Sun, Y., Zhou, X., Xiao, K., Xin, Q. (2024): Predicting time series of vegetation leaf area index across North America based on climate variables for land surface modeling using attention-enhanced LSTM. – International Journal of Digital Earth 17(1): 2372317.
[114] Xu, M., Zhang, Z., Wang, Y., Liu, B. (2023): Quantifying the contributions of climatic and human factors to vegetation net primary productivity dynamics in East Africa. – Frontiers in Forests and Global Change 6: 1332631.
[115] Xuan, W., Rao, L. (2023): Spatiotemporal dynamics of net primary productivity and its influencing factors in the middle reaches of the Yellow River from 2000 to 2020. – Frontiers in Plant Science 14: 1043807.

http://www.aloki.hu ● ISSN 1589 1623 (Print) ● ISSN 1785 0037 (Online)
DOI: http://dx.doi.org/10.15666/aeer/2402_31173147

[116] Yang, R., Wang, J., Zeng, N., Sitch, S., Tang, W., McGrath, M. J., Cai, Q., Liu, D., Lombardozzi, D., Tian, H., Jain, A. K., Han, P. (2022): Divergent historical GPP trends among state-of-the-art multi-model simulations and satellite-based products. – Earth System Dynamics 13(2): 833-849.
[117] Yılmaz, B., Aras, E., Nacar, S. (2024): A CMIP6-ensemble-based evaluation of precipitation and temperature projections. – Theoretical and Applied Climatology 155(8): 7377-7401.
[118] Yuan, W., Wu, S. Y., Hou, S., Xu, Z., Pang, H., Lu, H. (2021): projecting future vegetation change for Northeast China using CMIP6 model. – Remote Sensing 13(17): 3531.
[119] Yuxi, W., Li, P., Yuemin, Y., Tiantian, C. (2024): Global vegetation-temperature sensitivity and its driving forces in the 21st century. – Earth's Future 12(2): e2022EF003395.
[120] Zhang, H., Zhang, M., Jin, J., Fei, K., Ji, D., Wu, C., Zhu, J., He, J., Chai, Z., Xie, J., Dong, X., Zhang, D., Bi, X., Cao, H., Chen, H., Chen, K., Chen, X., Gao, X., Hao, H., et al. (2020): Description and climate simulation performance of CAS-ESM version 2. – Journal of Advances in Modeling Earth Systems 12(12).
[121] Zhang, L. X., Zhou, D. C., Fan, J. W., Hu, Z. M. (2015): Comparison of four light use efficiency models for estimating terrestrial gross primary production. – Ecological Modelling 300: 30-39.
[122] Zhang, P., Li, Z., Zhang, H., Ding, J., Zhang, X., Peng, R., Feng, Y. (2022): Simulation model of vegetation dynamics by combining static and dynamic data using the gated recurrent unit neural network-based method. – International Journal of Applied Earth Observation and Geoinformation 112: 102901.
[123] Zhang, S., Bai, Y., Zhang, J., Zheng, X., Ali, S., Ullah, H. (2024a): Intercomparison of gross primary productivity in spatio-temporal distribution over a typical tropical region based on different datasets. – Environmental Science and Pollution Research 31(50): 60650-60667.
[124] Zhang, S., Hao, X., Zhao, Z., Zhang, J., Fan, X., Li, X. (2023): Natural vegetation succession under climate change and the combined effects on net primary productivity. – Earth's Future 11(11): e2023EF003903.
[125] Zhang, S., Yang, S., Huang, J., Yang, D., Zhang, S., Zhang, J., Bai, Y. (2024b): Global-scale improvement of the estimation of terrestrial gross primary productivity by integrating optical and microwave remote sensing with meteorological data. – Ecological Informatics 83: 102780.
[126] Zhao, Y., Wang, L., Jiang, Q., Wang, Z. (2024): Sensitivity of gross primary production to precipitation and the driving factors in China's agricultural ecosystems. – Science of the Total Environment 948: 174938.
[127] Zhou, S., Zhang, Y., Ciais, P., Xiao, X., Luo, Y., Caylor, K. K., Huang, Y., Wang, G. (2017): Dominant role of plant physiology in trend and variability of gross primary productivity in North America. – Scientific Reports 7(1): 1-10.
[128] Zhou, Y., Zhang, R., Wang, S. X., Wang, F. T., Qi, Y. (2019): Comparative analysis on responses of vegetation productivity relative to different drought monitor patterns in Karst regions of southwestern China. – Applied Ecology and Environmental Research 17(1): 85-105.
[129] Zhu, W., Zhang, Z., Feng, S., Ren, H. (2024): Prediction and transition of vegetation vulnerability in the Mara River Basin under different Shared Socio-Economic Pathways (SSPs), East Africa. – Forests 15(4): 610.
[130] Zhu, Z., Piao, S., Myneni, R. B., Huang, M., Zeng, Z., Canadell, J. G., Ciais, P., Sitch, S., Friedlingstein, P., Arneth, A., Cao, C., Cheng, L., Kato, E., Koven, C., Li, Y., Lian, X., Liu, Y., Liu, R., Mao, J., et al. (2016): Greening of the Earth and its drivers. – Nature Climate Change 6(8): 791-795.

http://www.aloki.hu ● ISSN 1589 1623 (Print) ● ISSN 1785 0037 (Online)
DOI: http://dx.doi.org/10.15666/aeer/2402_31173147

APPENDIX

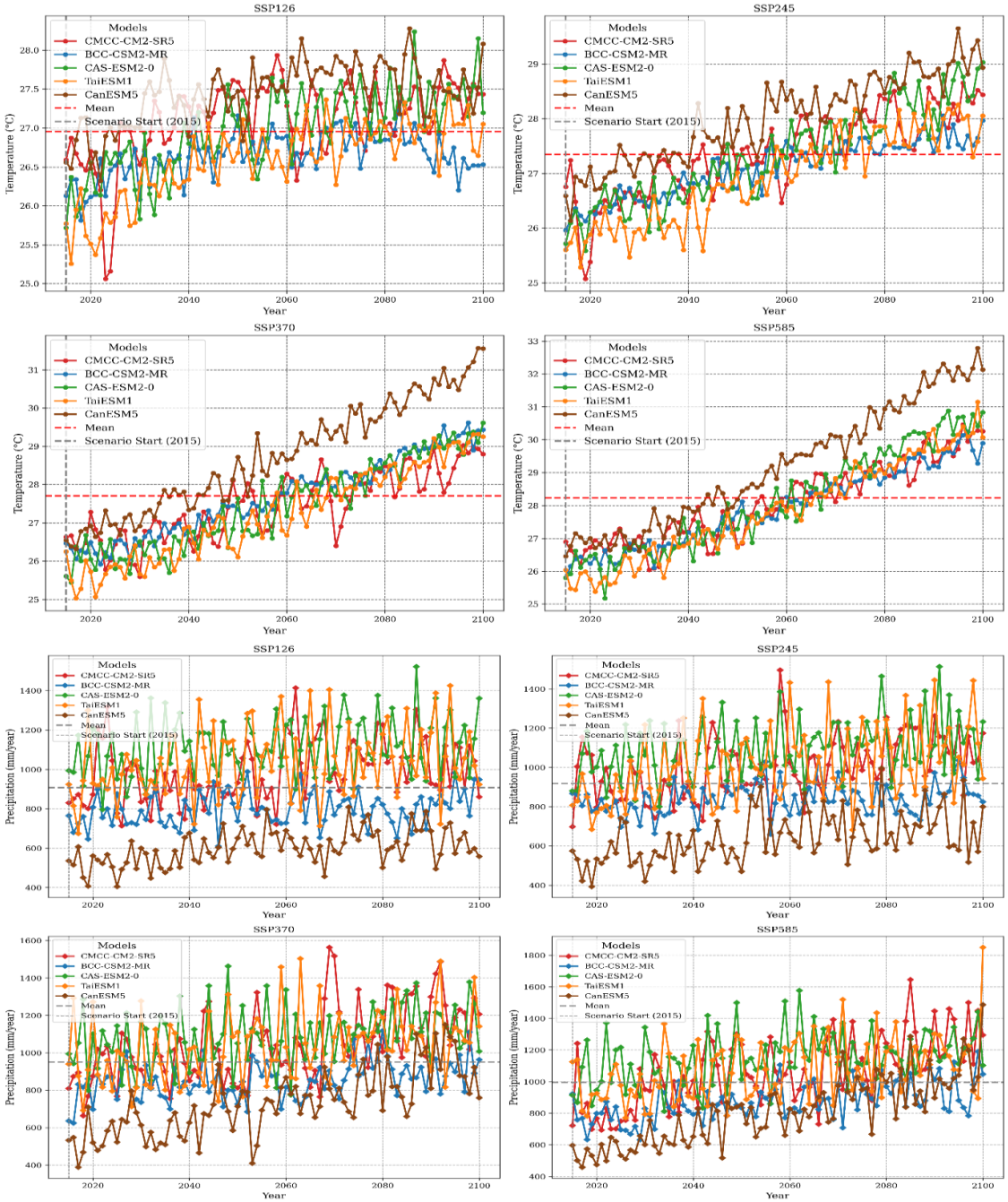

Figure A1. *Simulated temperature, precipitation and GPP multimodal ensembles mean (MEM) of ESMs models from 2015-2100*

http://www.aloki.hu ● ISSN 1589 1623 (Print) ● ISSN 1785 0037 (Online)
DOI: http://dx.doi.org/10.15666/aeer/2402_31173147

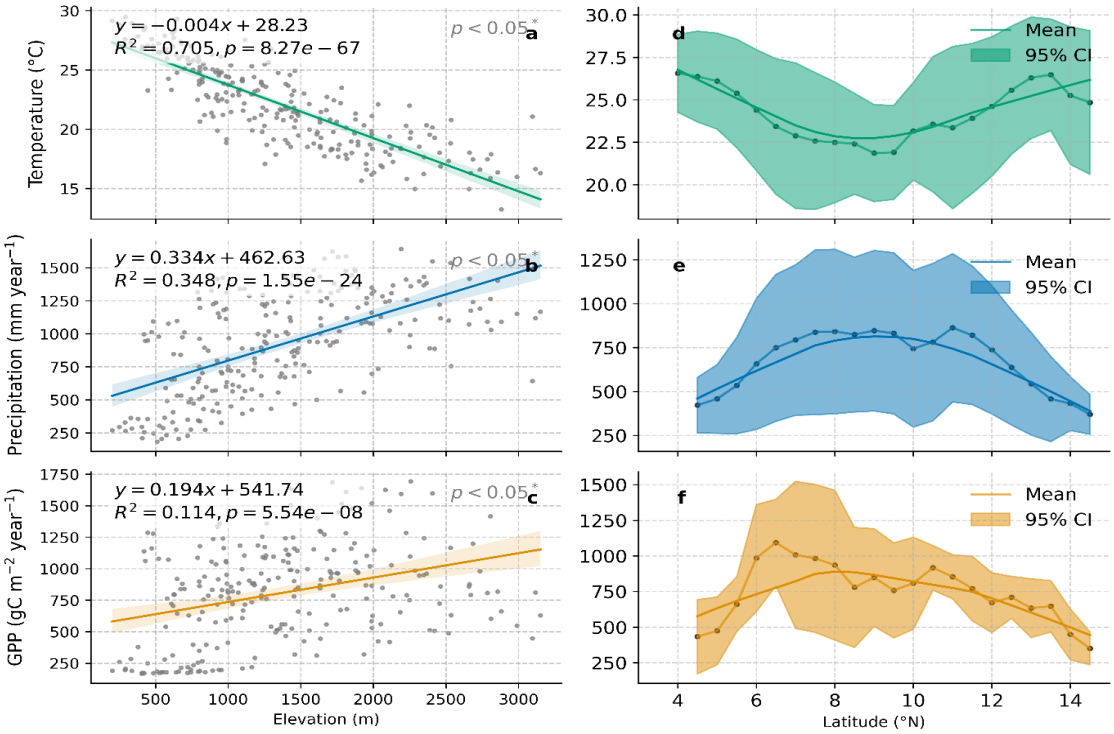

Figure A2. *Variation of climate factor temperature (a, d), precipitation (b, e) and GPP (c, f) across elevational and latitudinal difference, solid line represents trends of each variable*

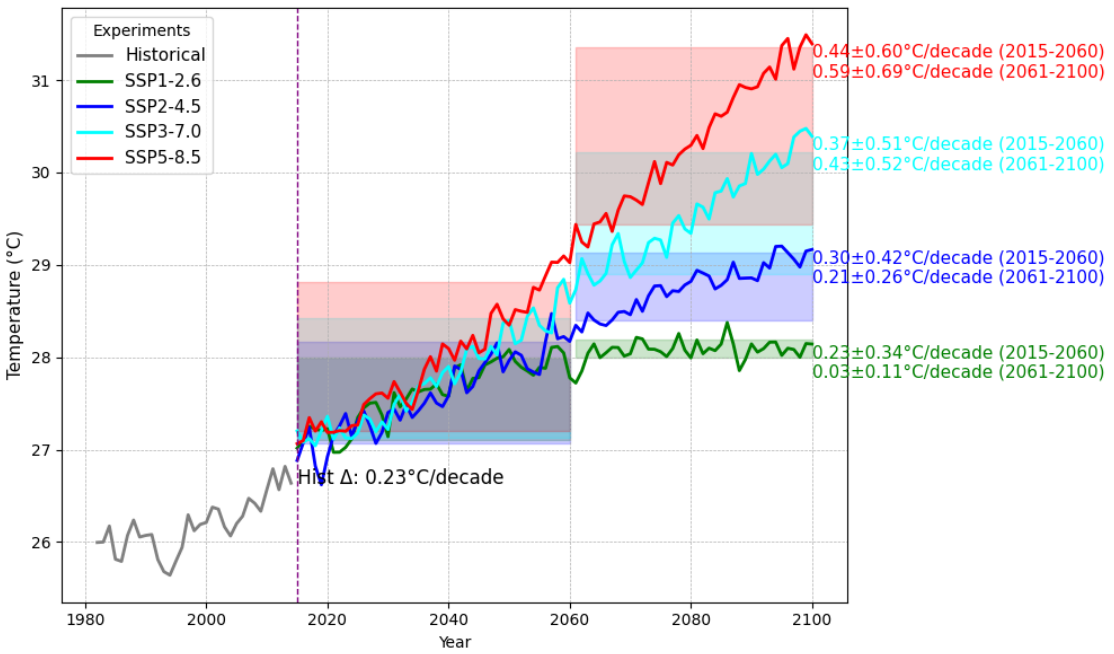

Figure A3. *Decadal variations of observed and future temperature value*

http://www.aloki.hu ● ISSN 1589 1623 (Print) ● ISSN 1785 0037 (Online)
DOI: http://dx.doi.org/10.15666/aeer/2402_31173147

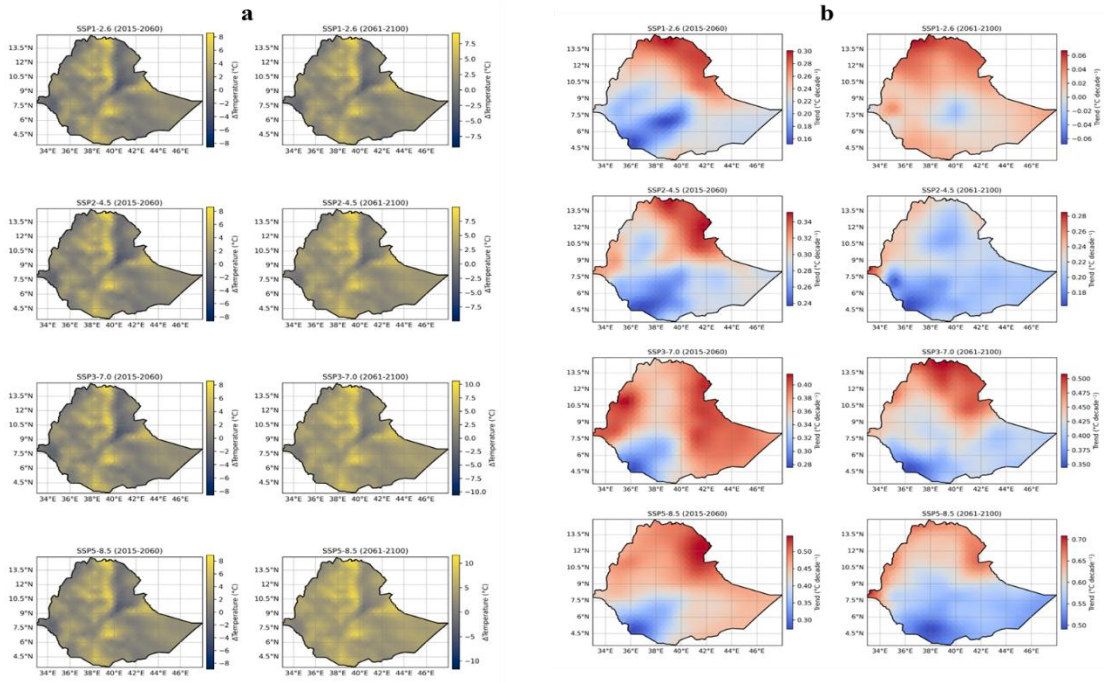

Figure A4. *The spatial distribution of annual mean temperature change (a) and trend (b) over Ethiopia in the near 2060(2015-2060) and far future 2100(2061-2100) period based on six ESMs in under SSPs scenarios*

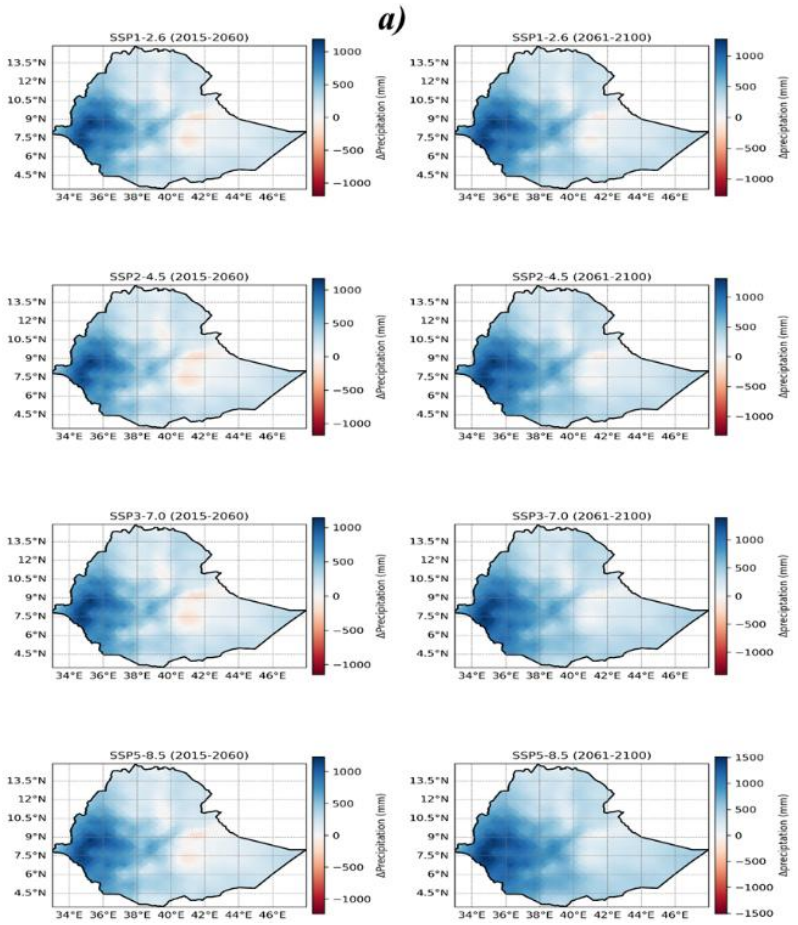

http://www.aloki.hu ● ISSN 1589 1623 (Print) ● ISSN 1785 0037 (Online)
DOI: http://dx.doi.org/10.15666/aeer/2402_31173147

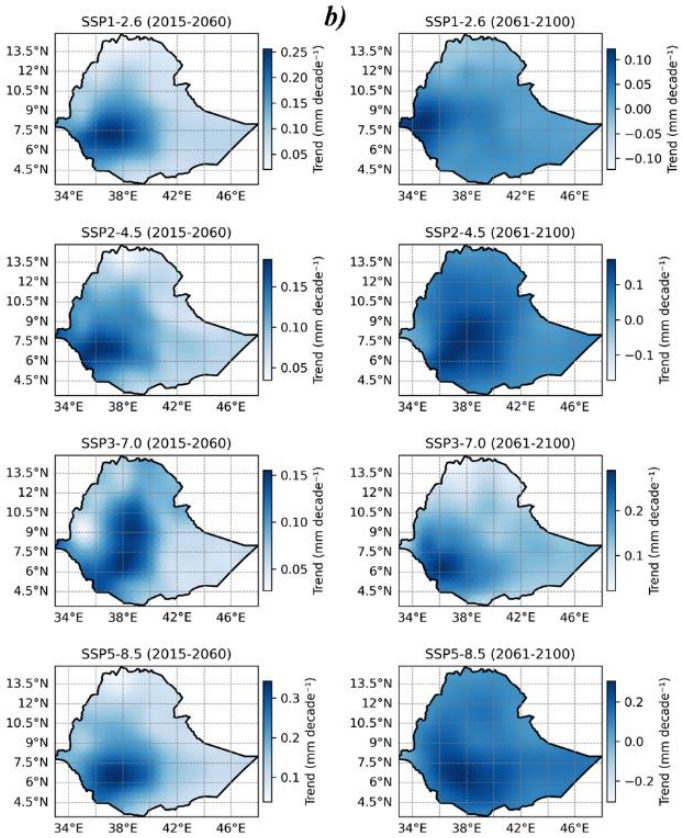

Figure A5. *Spatial average annual precipitation changes (a) and trends (b) between 1982-2014 and near future 2060, far future2100 from MEM of six ESMs under four SSPs scenario*

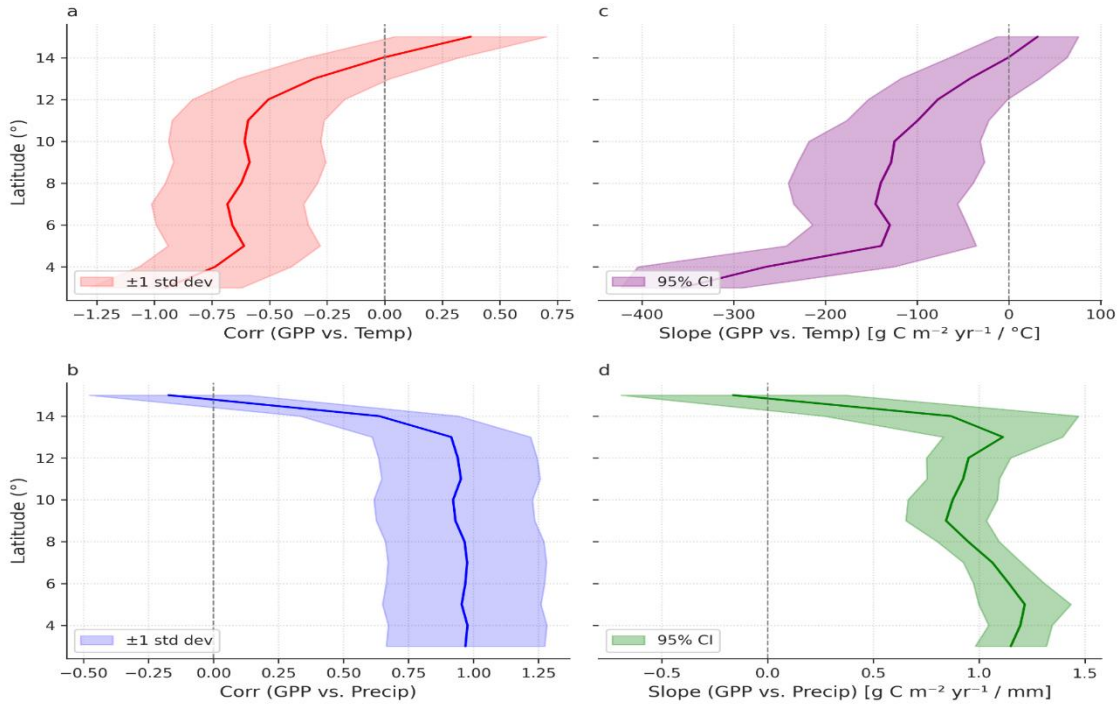

Figure A6. *Latitudinal variation of correlation and slopes between ensemble of future GPP and climate factors*

http://www.aloki.hu ● ISSN 1589 1623 (Print) ● ISSN 1785 0037 (Online)
DOI: http://dx.doi.org/10.15666/aeer/2402_31173147

Table A1. *Projected temperature likelihood to exceed 2°C under future scenario*

Scenario	2060 (ΔT°C)			2100 (ΔT°C)			2015-2100 (ΔT°C)		
	Decadal	**Projected**	**%**	**Decadal**	**Projected**	**%**	**Decadal**	**Projected**	**%**
SSP1-2.6	0.23 ± 0.34	1.03 ± 1.53	<5	0.03 ± 0.11	0.12 ± 0.43	<5	0.12 ± 0.35	1.02 ± 2.97	<5
SSP2-4.5	0.30 ± 0.42	1.35 ± 1.89	<5	0.21 ± 0.26	0.82 ± 1.01	<5	0.27 ± 0.69	2.30 ± 5.86	32
SSP3-7.0	0.37 ± 0.51	1.66 ± 2.29	6	0.43 ± 0.52	1.67 ± 2.03	7	0.41 ± 1.03	3.49 ± 8.75	80
SSP5-8.5	0.44 ± 0.60	1.98 ± 2.70	19	0.59 ± 0.69	2.30 ± 2.69	32	0.54 ± 1.36	4.59 ± 11.56	99

http://www.aloki.hu ● ISSN 1589 1623 (Print) ● ISSN 1785 0037 (Online)
DOI: http://dx.doi.org/10.15666/aeer/2402_31173147